A Fiducial Subject Pre-alignment System for the Biomedical Imaging and Therapy Beamline at the Canadian Light Source.

A Thesis

Submitted to the College of Graduate Studies and Research

In Partial Fulfillment of the Requirements

For the Degree of

Master of Science

In the

Division of Biomedical Engineering

University of Saskatchewan

Saskatoon, Saskatchewan

Canada

By

Aminat Adeola Popoola

PERMISSION TO USE

In presenting this thesis in partial fulfillment of the requirements for a Master's degree from the University of Saskatchewan, the author has agreed that the Libraries of this University may make it freely available for inspection. The author further agrees that permission for copying of this thesis in any manner, in whole or in part, for scholarly purposes may be granted by the professors who supervised this thesis work or, in their absence, by the Head of the Division or the Dean of the College in which this thesis work was done. It is understood that any copying or publication or use of this thesis or parts thereof for financial gain shall not be allowed without the author's written permission.

It is also understood that due recognition shall be given to the author and to the
University of Saskatchewan in any scholarly use which may be made of any material in this thesis.

Requests for permission to copy or to make other use of material in this thesis in whole or part should be addressed to:

Head of the Division of Biomedical Engineering
University of Saskatchewan
Saskatoon, Saskatchewan, Canada S7N 5A9

ABSTRACT

Positioning, immobilization, and organ motion are some of the major concerns in all imaging modalities. With synchrotron X-ray imaging, alignment of the region of interest to the beam is usually done inside the experimental hutch. However, because specimen alignment can be time consuming; such a system is wasteful of valuable beam time.

For the purposes of the Biomedical Imaging and Therapy (BMIT) beamlines at the Canadian Light Source, we propose an effective and versatile means of positioning a wide range of subjects (human and animal) with a wide range of sizes using a laser-based fiducial system to define the region of interest (ROI) before imaging; i.e., outside the experimental hutch. This system will allow the beam path through a specific region of interest to be modeled outside the imaging hutch in a way that it can be reproduced relative to the fixed X-ray beamline inside the hutch. The model will include an indication of the center of the beam and a rectangular area around the target delineating the limits of the area to be imaged (i.e., encompassing the "region of interest"). The rectangular field of view would be projected on the incoming (entrance) side of the subject as well as the outgoing (exit) side of the subject, and these projections must be coaxial with each other and parallel with the X-ray beam. This method is user friendly, allows mistake to be corrected before experiment and most importantly saves time.

ACKNOWLEDGEMENT

I would like to express my sincere appreciation to my supervisors, Dr. Gregg Adams and Dr Dean Chapman for their timely advice, constant guidance and thoughtful insights throughout the research. Special thanks to Saskatoon Health Region for the supply of the C-arm system used for the construction of the fiducial prototype. My appreciation also goes to the members of my supervisory committee, Prof. Daniel Chen and Dr.Tomasz Wysokinski. Many thanks to Chris Ryan at the Canadian Light Source for the provision of the MRTL drawing. My appreciations also to all members of the Engineering workshop for their timely help with the prototype construction, and to Kurtis Wanner for his assistance with the Solidworks software.

I appreciate the support and encouragement I received from my parents Alhaji and Alhaja T. A. Solagbade, my siblings, and from all my friends and colleagues. Financial assistance from NSERC grant to my supervisors is gratefully acknowledged.

Finally, my appreciation and special thanks to all those who contributed to the success of my M.Sc. Program. Thank you all.

DEDICATION

This thesis is dedicated to my darling husband, Haroun Akepola and my precious children; Abdur-Raqeeb Eniola and Yasmin Teniola for their love, support, encouragement and understanding throughout my course of study and always. I will forever love and appreciate you all.

LIST OF FIGURES

LIST OF EQUATIONS

LIST OF ABBREVIATIONS

AAFM	Angular Alignment Fiducial Mark
BE	Binding Energy
BM	Bend Magnet
BMIT	Biomedical Imaging and Therapy Beamline
CLS	Canadian Light Source
CT	Computed Tomography
DEI	Diffraction Enhanced Imaging
ESRF	European Synchrotron Radiation Facility
FM	Fiducial Marker
HXMA	Hard X-ray Micro Analysis Beamline
ID	Insertion Device
KES	K-edge Subtraction Imaging
MPAP	Mouthpiece Attachment Plate
MRI	Magnetic Resonance Imaging
MRT	Microbeam Radiation Therapy
NSLS	National Synchrotron Light Source
PAT	Photon Activation Therapy
PCI	Phase Contrast Imaging
PET	Positron Emission Tomography
PGM	Plane Grating Monochromator
REIXS	Resonant Elastic and Inelastic X-ray Scattering
RF	Radio Frequency

ROI	Region of Interest
SGM	Spherical Grating Monochromator
USAXS	Ultra –Small Angle Scatter Rejection
VUV	Vacuum Ultraviolet

TABLE OF CONTENTS

1 Introduction

1.1 Overview

In medical imaging and therapy, several methods have been used for target alignment to the beam or beam alignment to the target using some form of fiducial system, and each of these methods depends on the type of imaging modality [1].

A fiducial is defined in medical imaging as an object used to create a reference point or landmark on a subject, to provide a 2, or 3-dimensional reference image of the anatomical site they are attached to [1, 2]. There are two types of fiducial methods use in medical imaging and therapy; these are the invasive and non invasive methods. An invasive method involves the break of the internal body cavity beyond the body orifice and inserting the fiducial on the anatomic site, while the non-invasive is a movable object placed external to the body and conform to the structure / shape of the target. [3]. However, in synchrotron imaging the most common fiducial method is based on a set of lasers which are aligned to take the same beam path as the X-ray beam inside the hutch. In most cases, this method may require as much or more time as the actual image acquisition and therefore represents an important inefficiency in the use of beam time [4].

In all synchrotron facilities, one of the fundamental challenges facing medical imaging is the use of the experimental time for specimen positioning/alignment inside the hutch. Therefore there is a need for an effect and versatile means of subject pre-alignment outside the hutch and a fiducial pre-alignment method which will be placed remote to the imaging has been proposed to address this issue and the method is discussed in this thesis.

The main objective of this thesis is to:

(1) Give a survey on conventional methods as well as on the synchrotron imaging modalities proposed on the biomedical imaging and therapy beamlines (BMIT) at the Canadian light Source (CLS).

(2) Discuss and compare current fiducial methods used in medical imaging and therapy and their limitations.

(3) Reduce the time it takes to align subject in the biomedical beamlines.

(4) Provide a way of subject alignment that is more natural to medical community.

This thesis is divided into six (6) chapters to address these objectives: Chapter 1 gives a brief introduction of the thesis, discusses some conventional X-ray methods, and highlights some synchrotron imaging and therapy methods. Chapter 2 discusses different fiducial methods use in medical imaging. Chapter 3 focuses on the proposed fiducial system for the BMIT beamlines. Chapter 4 explains the C-arm fiducial system, the MRT-lift and the transformation methods used for the proposed fiducial system. Chapter 5 discusses the simulation results and performance analysis. Chapter 6 is the concluding chapter and discusses the future work.

1.2 Medical Imaging

An image can be defined as a two or three-dimensional reproduction of an object or scene. It can be analyzed or processed using image processing systems to help recognize certain features, improve visibility or display digital information for quantitative analysis [5]. In medical imaging, different imaging methods may be employed to examine a particular tissue or organ of interest in a subject, and each of these methods may reveal different characteristics of the region. Two image properties, Structure visibility and Image quality are mostly considered when deciding on any type of imaging method for querying an anatomic region; this is because the visibility of an anatomical feature depends mostly on the properties of the imaging modality, and how it is operated [6]. To achieve optimal image quality, certain components of the imaging modalities may be changeable, such as intensifying screens in radiographic imaging, transducers in sonography, or coils in magnetic resonance imaging while other components may be adjustable, such as kilovoltage in radiography, gain in sonography and echo time in magnetic resonance imaging. The image is then analyzed using different processing tools available for each modality to improve the image quality. Other image properties that can also be considered are the image resolution, unsharpness and/or signal-to- noise ratio of the imaging modality. Some medical imaging modalities are discussed in the sections that follow.

1.2.1 X-ray radiographic imaging

X-ray production

X-rays are high-energy photons, similar to ordinary visible light but with more energy and a shorter wavelength. The wavelength of X-rays varies from about 10 *nm* for low energy radiation, to about 10^{-4} *nm* for high energy X-rays. A conventional X-ray tube consists of a filament, which is heated to emit electrons by thermionic emission, and a tungsten target, which is positively charged with respect to the filament. Tungsten atom is used as a target because it can withstand bombardment; it has a high melting point, and can conduct heat away. There are two types of electron-atom interactions that will result in the production of X-rays, line or characteristic radiation and Bremsstrahlung or “braking” radiation (also called the continuous spectrum) [5, 7].

Characteristic Radiation

Every atom consists of negatively charged electrons that circle around the positively charged nucleus. The nucleus consists of protons and neutrons, and is where the majority of mass is concentrated [8]. The electron orbits are grouped into shells and there are a maximum number of electrons that can occupy a given shell. The innermost shell is referred to as the K-shell and has a maximum of 2 electrons, the next (L-shell) has 8 electrons, the next (M-shell) has 18 electrons, and the next (N-shell) has 32 electrons [8]. Characteristic radiation is produced by an ionization process which arises when the negatively charged electron from a cathode interacts with the electrons of a target atom. The incoming electron removes an electron from the atom, thereby creating a “hole” in the electron shell. The target atom becomes unstable and the hole is quickly filled by the next available electron from an adjacent outer shell. If a K-shell electron is removed, an electron from the outer shell fills the electron hole, resulting in the production of a characteristic X-ray photon with energy equal to the difference between the binding energies (BE) of the electrons involved. The energy of the X-ray produced if a K-shell electron is ionized, and its hole is filled by an L-shell electron is calculated as below:

Energy of the X-ray = Binding energy of L-shell - Binding energy of K-shell

Where Binding energy of K-shell = -12.1 *keV* and Binding energy of L-shell = 57.4 *keV*.

Although, M X-rays, N X-rays and O X-rays can be produced by the ionization process, the K X-rays are more useful in imaging because it has an average energy of 69 *eV* which falls within the range of energy use in medical imaging (15-100 *keV*). This is one of the reasons why characteristic radiation is sometimes called the K-shell emission [8].

The Continuous spectrum (Bremsstrahlung) radiation

Continuous spectrum radiation is produced as a result of the interaction of an incoming electron with the nucleus of an atom. The incoming electron penetrates the atom's electron "cloud" and gets closer to the nucleus; it is influenced by the electrostatic field of the nucleus. The electron undergoes changes in direction and dramatic reductions in speed and kinetic energy. The energy that is lost during the process is emitted as high energy X-ray photons, known as Bremsstrahlung X-rays. The amount of photon energy emitted depends not only on the amount of collisions but also on the amount of energy the electron retains after collisions. The electron may lose all its energy in a single collision or it may retain some for subsequent collisions with other electrons, both resulting in X-ray photon emission with energy ranging from 0 to the highest kilovoltage [7, 8]. Low energy photons are produced by the "braking" process when the incoming electron is influenced only slightly by the nucleus, while high energy photons are produced when the incoming electron loses all of its energy and comes to rest [8]. The energy of emitted photons is expressed as:

$$E = eV \qquad \text{Equation 1.1}$$

where E = Electron energy = Photon Energy

e = Electronic charge

V = Tube voltage.

If expressed in terms of wavelength the photon energy is:

$$E = eV = hv = h\frac{c}{\lambda} \qquad \text{Equation 1.2}$$

where h = the Planck's constant

v = Frequency

c = The velocity

λ = The wavelength of the emitted photon [6].

1.2.2 Computed Tomography

Computed tomography (CT) is a cross-sectional imaging technique which produces serial planar views through the subject that can then be viewed as individual 2-dimensional "slices" or concatenated to provide a 3-dimensional image. While conventional projection radiography may be used to achieve sub-micron resolution, it provides limited information for soft tissue because of the inability to detect a small linear absorption coefficient without the use of a contrast agent. The X-ray CT modality uses a computational method to convert projection images into both 2-dimensional and 3-dimensional data sets to produce volumetric information for anatomical and functional analyses. Drawbacks of CT include the increase in data acquisition time due to the number of image slices required, and the increase in patient exposure time which increases patient X-ray dose [9].

1.2.3 Contrast Imaging

1.2.3.1 Phase Contrast Imaging

Contrast is produced from variations in X-ray absorption from different parts of a sample [9]. Samples with higher atomic number absorb more X-rays while those with a lower atomic numbers absorb less. Soft tissues of the body contain mainly carbon, nitrogen, oxygen and hydrogen, all of which are weak X-ray absorbers because of their low atomic number. Hence, soft tissues provide poor image contrast. An approach to increase contrast in soft tissues is to use a contrast agent, such as iodine or xenon. Unfortunately these contrast media produce other adverse effects during administration [9]. The best approach that can be used is one that will deliver a small dose of damaging X-rays, yet will provide good contrast. One such method is called phase contrast imaging (PCI) which involves the property of diffraction rather than absorption to generate an image.

This diffraction technique uses an X-ray interferometer consisting of two crystal blocks. This method splits (diffracts) the X-ray beam into two so that one path of the beam is directed to the object and the other part is used as the reference beam. X-rays that satisfy diffraction condition and that are in lattice plane perpendicular to a crystal wafer are divided into two and later discharged from the back of the wafer. The reference beam that is produced as a result of the division is again divided by the second wafer and at the back of the second wafer the two beams are brought together while the third wafer mixes the two beams together to produce an interference pattern. After the production of the interference pattern, the next step is to measure the X-ray phase which is achieved by measuring all the interference patterns by an image sensor and then convert the patterns to an image that maps the distribution of the X-ray phase shift such as a 3-D image which could be seen as a physical image using the process of phase map.

The major advantage of PCI method is that it may reveal structures in weakly absorbed objects such as soft tissues than in conventional method because of its increase in contrast sensitivity. It improves diagnosis reliability by detecting tumor at early stage with the ability to distinguish between malignant and benign growths [9].

1.2.4 Positron Emission Tomography

PET is another tomographic imaging technique like CT and MRI. Positively charged positrons are produced by some radioactive isotopes such as Oxygen 15, Carbon, and Fluorine 18. These isotopes annihilates with negatively charged electrons in biological tissues to produce an annihilation radiation of approximately 1 *MeV* [10, 11]. Due to high electron density in biological tissue, there is continual interaction of the electrons and the isotopes which will eventually result in the disappearance of the two particles and both replaced with two gamma rays. Because of this continual interaction, many projected data produced are used in the reconstruction of the isotope concentration. There are many advantages of PET in clinical diagnostic studies, because it can easily detect subtle pathologies due to its high sensitive of its detector to radioisotope elements [10].

1.2.5 Synchrotron imaging

Synchrotron light is produced as a result of charged particles such as electrons moving at a relativistic speed in a magnetic field of a bending magnet and forced to move in a circular orbit or in an insertion device such as undulators or wiggler. If the electrons are forced to move at a relativistic velocity, they emit synchrotron radiation in the forward direction and at a tangent to the orbit, whereas if the electron moves at a non-relativistic velocity for example in a linear accelerator, the electron is accelerated in the same direction as it travels and the energy loss to radiation is negligible and could not be converted to synchrotron radiation [13, 14]. Therefore, for the emission of photon energies ranging from infra-red to energetic X-rays, high-energy electron or positron storage ring are used [14]. Another important factor is the power the electron radiates at both relativistic and non-relativistic velocities. At relativistic velocity, the power radiated is expressed as [13].

$$P = \frac{2}{3}\frac{e^2\gamma^2}{m_0^2 c^3}\left|\frac{dp}{dt}\right|^2 \qquad \text{Equation 1.3}$$

where m_0 the rest mass of the particle

e is the electron charge,

c is the speed of light

$p = m_0 v$, is the momentum $(1/m_0)$,

(dp/dt) is the acceleration

γ is the ratio of mass.

$$\gamma = \frac{E}{m_0 c^2} = \frac{1}{\sqrt{1-\beta^2}}, \quad \beta = \frac{v}{c} \qquad \text{Equation 1.4}$$

If moving at a non-relativistic velocity, $\beta \sim 0$ and γ =1. Therefore, the radiated power is

$$P = \frac{2}{3}\frac{e^2}{m_0^2 c^3}\left|\frac{dp}{dt}\right|^2 \qquad \text{Equation 1.5}$$

Based on the above equations, the radiated power depends on the angle between the direction of motion of the electron and the direction of the acceleration, and also on the energy of the particles [13]. The machine that helps in the production of this photon is the storage ring but commonly called the synchrotron. The synchrotron machine works with different other machines to produce the synchrotron radiation; these are the linear accelerator, the radio frequency (RF) cavity, the storage ring itself, and the insertion devices (wiggler and undulators).

The linear accelerator and the booster synchrotron work together to speed up the electron to the desired energy of the storage ring before it is injected into the storage ring by injection devices such as pulsed magnets, (which is an inflector that bends the electron into the storage ring). If the storage ring is of low energy, instead of using the linear accelerator for pre-acceleration a “microtron” miniature electron accelerator is used. The RF cavity, which is at a straight section bundles the electrons into the storage ring within a time range of nanosecond to microsecond and it, also refills the energies loss by the electrons in the storage ring [13].

The storage ring is a tube that’s made up of a symmetric straight and bending sections of aluminum or stainless steel tubes under ultra high vacuum and it comprises of different other devices such as the magnetic devices with “focusing”, “defocusing” and “bending capabilities”, which are positioned to confine the electrons in a prescribed orbit. The bending magnets are placed in the curved sections of the ring to produce a dipole radiation with continuous spectral distribution, and the sextuples are used to keep electron energies at their preferred values [13].

The third generation synchrotron brought about the usage of insertion devices (ID) known as the wigglers and the undulators and some hybrid versions, which are installed in the straight sections of the storage ring. Their main function is to produce still brighter beams. A wiggler uses short period of magnets with large magnetic field that gives the electrons a sizable bend as they navigate through it, thus producing a range of radiation that nearly equals to the radiation of the bending magnet. Undulators on the other hand are very flexible and can produce powerful brightness at both Vacuum Ultraviolet (VUV) and X-ray range. The most important parameter of both insertion devices is the strength parameter K, expressed as

$K=0.934\,\lambda_U\left[cm\right]B_0\left[T\right]$ [26] Equation 1.6

where λ_u is the duration, B_0 is the peak magnetic field.

1.3 Background

1.3.1 The Canadian Light Source

Synchrotron light is produced as a result of charged particles such as electrons moving at a relativistic speed in a magnetic field of a bending magnet or an insertion device. The beam produced through this means is many times brighter than sunlight and it ranges from far infra-red to hard X-rays regions. To examine any sample or material using this beam, the desired wavelength of the beam is selected, and then transfers into the beamline and to the experimental hutch where sample analysis occurs. Unlike Conventional X-ray, the beam from synchrotron source is monochromatic, highly polarized, intense and tunable. These unique characteristics make imaging bone and soft tissues with lower radiation dose possible. At the Canadian Light Source there are about 14 beamlines which are grouped into phases based on their operational dates, out of these; two beamlines have been dedicated mainly for medical imaging and therapy purposes. The two beamlines are Biomedical Imaging and Therapy Beamline (BMIT-BM & ID.) They are to be used for synchrotron imaging and therapy on Human, Animals and Plants [15].

1.3.2 The Biomedical Imaging and Therapy Beamlines

The beamlines which are reserved for medical Imaging and Therapy at the Canadian light Source are from both bending magnet (BMIT-05BM) and insertion device (BMIT-05ID) sources. The BMIT-05ID is the primary source for the imaging and therapy capability of the facility. The beam from this source is intended to be used on various size subjects such as animals (from horses to rodents), plants and human subjects, for this purpose, a uniform fan beam high and wide enough to cover this subjects range is needed, the scan area of this beam is estimated to be approximately 20 cm wide and 30 cm high from the source point. It would be used to carry out different imaging and therapy modalities ranging from Conventional Imaging, Diffraction Enhanced Imaging (DEI), Multiple Imaging Radiography (MIR), K-edge Subtraction (KES), Computed Tomography (CT), CT Therapy and Microbeam Radiation Therapy (MRT) [16]. Since these imaging techniques require varying photon energies and fluxes a superconducting wiggler with a magnetic field strength of about 4 T, critical energy of 22.37 keV with a period of 4.8 cm and a deflection parameter K of 17.93 is used as the insertion device. For imaging purposes, the subject is expected to be located at about 50 m i.e. (±2 milliradians or $\pm 0.63K/\gamma$) from the source and this brings the critical energy down to 17.31 *keV*. For radiotherapy purpose, specifically Microbeam Radiation Therapy (MRT), with dose being one of the major factors, therefore wiggler with a pole number of 24, that will generate approximately 24*kW* power and deliver 2500 *Gy/s* is proposed [17, 16]. The BMIT-05BM is added to increase the imaging capability of the insertion device source by carrying out other therapy and imaging techniques such as photon activation therapy, X-ray scatter imaging, small angle X-ray scattering, phase contrast or in-line holography and ultra small angle scattering of DEI/MIR. Like all other bend magnets at the CLS its bending radius is about 7.144 *m* with field strength of 1.354 *T* and a critical energy of 7.57*keV*. It has a spectral brightness approximated to $3.7 \times 10^{13}\, photons/s/mrad^2/0.1\%bw$ at 20 *keV*. At a source distance of 30 *m*, flux K is estimated to be about $4 \times 10^9\, photons/s/mm^2$ if the beam is tuned with (Bragg) double crystal monochromator [16, 17]. Figure 1.1 shows the comparison between CLS superconducting wiggler and the ESRF wiggler.

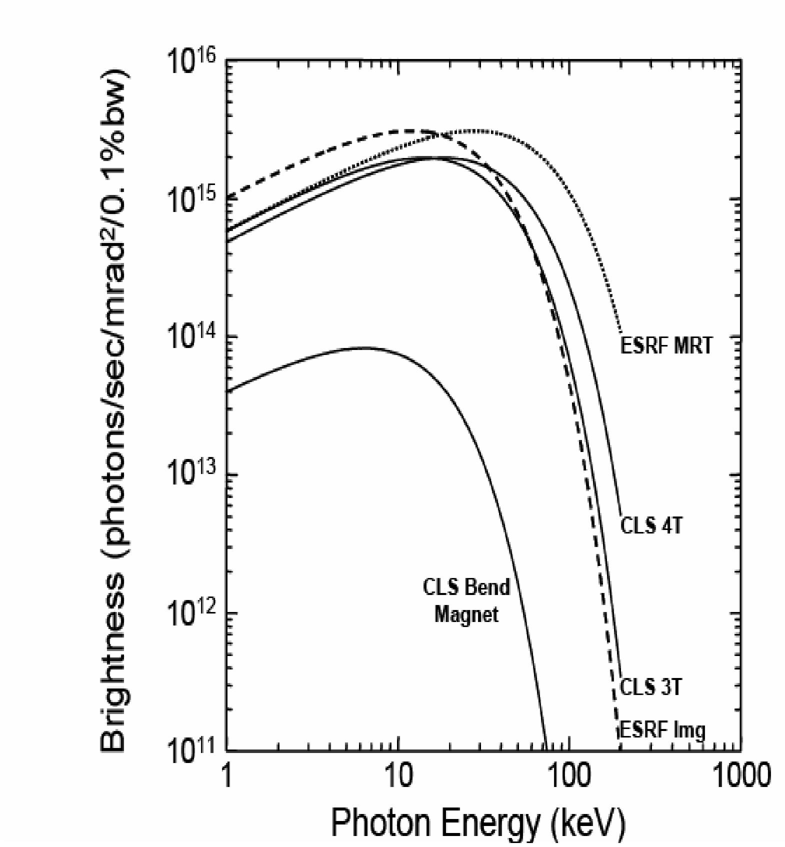

Figure 1.1 Comparison of the proposed CLS BMIT –ID superconducting conducting wiggler (*12poles, 500 ma. 2.9 GeV*) at *4T* and *3T* maximum field with the ESRF ID17 wiggler operating at (*6 GeV, 200 mA, and 11 periods*) for *1.4T* maximum field MRT and imaging with *0.6T* max field. The dotted line shows the ESRF (MRT) and the dashed line shows the ESRF imaging techniques [17].

Modalities on BMIT Beamlines

The BMIT – ID has several photon characteristics which makes it ideal for different imaging modalities, it has an operating energy range of 20-100 keV , it’s wavelength is between 0.6 – 0.1 $\AA$ and resolution that spans various modalities with DEI operating at resolution of 10-5 , and a spot size of 200 mm x 10 mm [17] . With its operation around the corner, several imaging techniques to be experimented on this beamline have already been proposed and are discussed in the next few chapters.

1.3.2.1 Imaging

(a) Absorption Imaging

In imaging, “everything is all about contrast” [18]. Contrast is the relative variation of image property. To achieve a reasonable contrast, the intensity of the beam must be high enough, which in turn increases the signal –to –noise ratio [18, 19]. For health reasons, there is maximum allowable radiation dose, which may be given at a time. There are two basic methods by which good contrast may be achieved in medical imaging, either by changing the intensity or phase of the incident photon as it transverses the object, or through the scattered radiation produced from the incident beam as it transverses a matter such as in Compton scattering. The latter results into two major contrast achievement, a volume element image as a result of using beam of isotropic intensity, or tomographically reconstructed image due to beam of wider angular range [19].

The monochromacity nature of synchrotron beam, its tunability, and high intensity make synchrotron absorption imaging of greater advantage than the conventional absorption method. Absorption imaging using synchrotron on the BMIT beamline will optimize a highly tunable and monochromatic beam of energy to penetrate variations of subject thickness in order to produce valuable results for the researchers and the clinicians. The beamline will make use of the variation in absorption at the K-edge of some elements to produce the K-edge subtraction imaging method, which may be used to study coronary arteries as in coronary angiography; KES will also be combined with high resolution camera to investigate small vessels to study problems in the heart and brain. Other advantages of the absorption imaging technique would also be utilized to carry out computed tomography imaging technique (CT) [16, 17].

*(b)*K-edge Subtraction (KES)

A method of absorption technique that has been proposed for the BMIT beamlines is the K-edge subtraction method. This method is used to reduce the artifact caused as a result of anatomical motion in conventional subtraction imaging technique. Conventional imaging method involves a process of first imaging a target without the injection of a contrast agent while a second image of the same target is taken by injecting a contrast agent such as (xenon, iodine e.t.c) then image at energy just above the absorption energy of the contrast element. Subtracting these images gives a map of the contrast medium. The major limitation to this method is poor image quality, which is as a result of organ movement during imaging. Using KES method for subtraction imaging, the synchrotron from the source is diffracted by a bent Laue crystal to produce energies below and above the absorption edge of contrast agent. These energies are applied simultaneously to the target and the energy above the edge produces image information due to Compton and photoelectric effects, while the energy below the edge is mainly through Compton scattering [17, 19, 20]. The two images are logarithmically subtracted to produce maximized image of the contrast medium [19, 20] The KES method showing the photoelectric absorption effect of xenon, soft tissue and bone is as shown below.

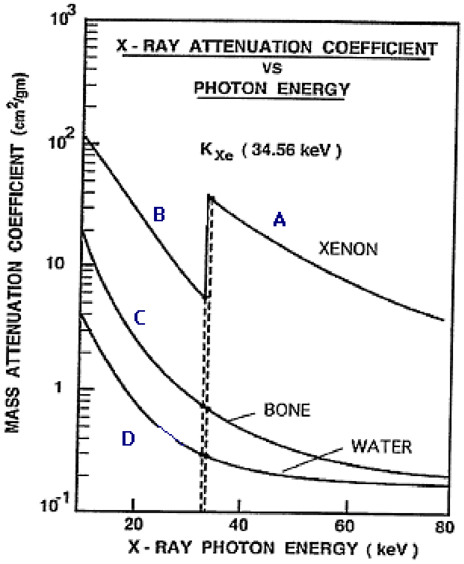

Figure 1.2 The attenuation of X-ray as a function of Energy. Curve A shows the attenuation by xenon. Curve B the attenuation by soft tissue and Curve C the attenuation by bone. As shown, there is an increase in attenuation of Xenon as the energy approaches 34.56 keV [20].

(c) Coronary Angiography

This is one of the KES diagnostic imaging methods that would be carried out on the BMIT beamline. It is an examination of the blood vessels using photons in the X-ray region. During the procedure, the patient is positioned motionless with their hands on their sides or over their head. The process involves inserting a tip of a catheter in the heart or into the arteries supplying the heart and injecting a contrast medium with iodine composition to take the angiograms. Following this process KES technique is applied in order to eliminate the (arterial catheterization) complications caused by the conventional method as well as obtaining image of high quality [19, 21]. Figure1.3 shows the mouse coronary angiography method at the Japan Synchrotron Research Institute.

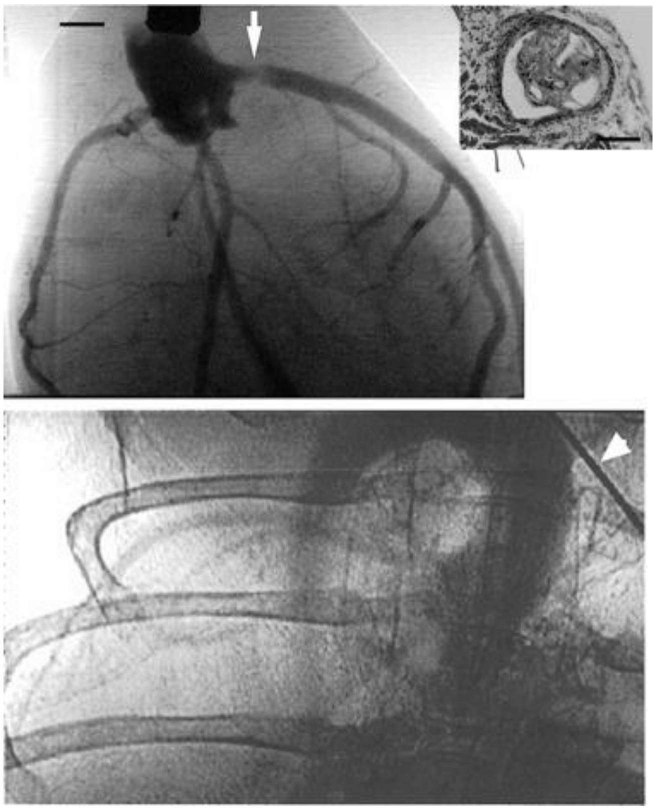

Figure1.3 Image of mouse coronary angiography using synchrotron radiation micro- angiography performed at the Japan Synchrotron Radiation Research Institute, Harima, Japan. The top shows a coronary angiography from an apolipoprotein E mouse fed with a high cholesterol diet for 5 months. At the proximal end of the left coronary artery, a severe steno tic lesion was detected (arrow). The top-right shows the histological analysis of the stenotic lesion. While the bottom shows, in-vivo coronary angiograph of an anesthetized C57BL/6 mouse [21].

(d) Micro angiography

This diagnostic method is similar to coronary angiography but it goes further to investigate any blockage in the heart and the brain by using high resolution camera to visualize the tiny vessels. This method has been proposed to be carried out on the BMIT beamline [19].

(e) Computed Tomography (CT)

CT is a cross-sectional imaging technique that shows the attenuation property of an X-ray as it transverses through the body. The major disadvantage of the conventional CT method is inability to interpret the image quantitatively due to change in attenuation caused by beam hardening. The high tunability and collimation characteristics of X-ray from synchrotron source erase the beam hardening effects. Monochromatic property of synchrotron beam at the CLS would be employed in dual/multi CT to distinguish between low and medium Z- elements. Also a pencil beam from the source would be used in fluorescence CT to generate a fluorescence signal, which may be used in in-vivo for imaging non-radioactive elements. The only set back with synchrotron method is that the beam is stationary so the object has to be rotated at 90 degree along the fan-beam plane [10, 19, 22].

(f) Diffraction Enhanced Imaging (DEI)

This is one of the main radiographic methods that would be carried out on the BMIT beamline at the CLS with energy of about 100keV and resolution reduced to approximately $50\mu m$. It is a technique that produces absorption, refraction as well as extinction contrast mechanisms [10, 19, 22]. In DEI experiment a collimated beam from a monochromatic crystal traverse through an object and a single silicon analyzer crystal similar to the monochromatic crystal is made to analyze the beams that impinge upon it. This analyzer crystal can be set on each side of its reflectivity curve to produce two types of image namely the refraction angle image and the apparent absorption image. Absorption contrast mechanism is determined by integrating the intensity of the distribution on each image pixel. Refraction image is determined from the analyzer crystal, by locating the centre of the angular distribution on each image pixel while extinction image (MIR technique) an extension of DEI technique can also be determined by locating the width of the angular intensity distribution which is by calculating the variance of the intensity distribution [23, 24, 25]. At NSLS X15A imaging beamline, (D. Chapman et al) have carried out an experiment on human cadaveric foot to show these contrast mechanisms. These images were produced by varying the analyzer crystal at 40keV, and positioning the monochromatic and analyzer crystals in parallel with a mean exposure of 0.12mGy per image. The images obtained using MIR method are as shown in Figure 1.5 [25, 26].

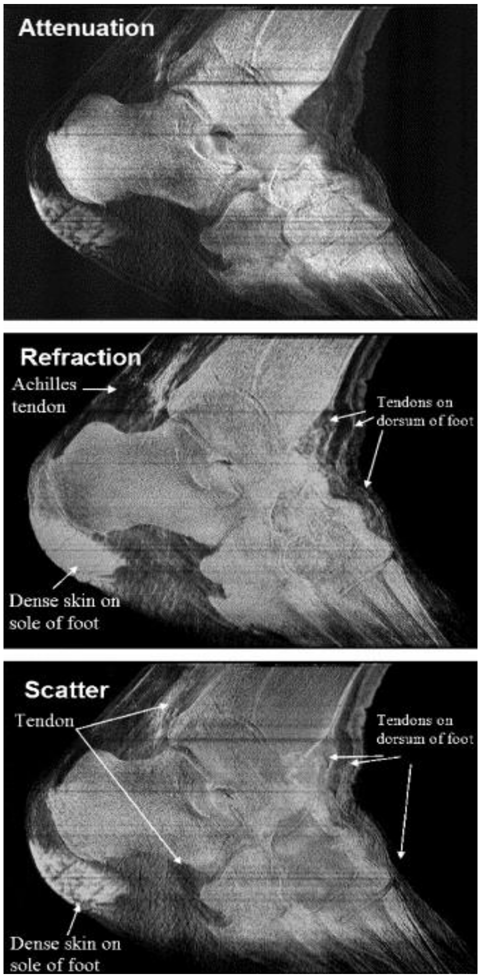

Figure 1.5 The top image shows the attenuation i.e. absorption image.

Figure 1.4 The top image shows the attenuation i.e. absorption image. The middle image is the refraction mechanism. The bottom shows the Extinction mechanism. From the diagram, it can be deduced that soft tissues can easily be visualized with refraction and extinction techniques while absorption shows well only the calcified soft tissues [25].

(g) **Multiple Image Radiography**

This technique described by [26] is an improvement of the DEI technique. It corrects the errors in DEI and it is more susceptible to noise. While DEI produces multiple parametric images i.e. apparent absorption and refraction images, MIR produces three distinct images of absorption, refraction and extinction (Ultra –Small-angle-Scatter-Rejection (USAXS)) images. The setup of MIR is the same as with DEI and generation of each contrast techniques is the same. Both DEI and MIR may be used to image at high energies and still minimizing the risk to the patient by lowering radiation exposure. Both techniques can also display calcified and soft tissues simultaneously [25].

1.3.2.2 Radiotherapy on the Biomedical Beamline

The CLS biomedical beamline will carry out various radiotherapy techniques by employing some of the characteristics of the beam generated from the insertion device and the bend magnet. The high collimating beams generated through these means will be used to target small tumors while the tunability property of the beam will make the beam able to penetrate the tumor to a particular depth. The monochromaticity of the beam will also eliminate beam hardening effects as well reduce Compton effects considerably. At the CLS the radiotherapy techniques that will be experimented on the BMIT beamline are [19, 24].

(a) **Microbeam Radiation Therapy (MRT)**

A therapeutic technique first discovered at the National Synchrotron Light Source (NSLS) Brookhaven is aimed at reducing damaged tissue necrosis developed during conventional radiation therapy [27]. To achieve this, the beam is divided into smaller spatially separated parallel Microbeam separated by about $100-200\mu m$ [16]. The target is positioned to ensure that it receives enough collimated beams that cross it at different locations and only micro fractionated dose is received by the surrounding healthy tissues as illustrated in Figure 1.7 [24]. This theory works only if there is sufficient undamaged volume of healthy tissues by which the damaged cells may regenerate. The main limitation to this technique is that it can be carried out only at certain synchrotron facility that can generate the Microbeam, with CLS BMIT beamline one of such facilities.

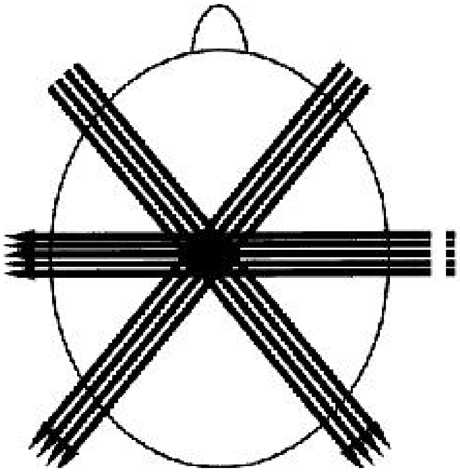

Figure 1.6 An illustration of spatially micro fractionated dose to surrounding healthy tissues [24].

(b) CT Therapy

The main purpose of this therapy technique is to reduce the amount of dose received by healthy surrounding tissues by administering the dose in tomographic mode to target tumor cells. The process is such that a contrast medium such as iodine is injected in the target volume and a monochromatic crystal is use to deliver a beam of energy above the K-edge of the contrast agent to the tumor volume [19] .

(c) Photon Activation Therapy (PAT)

This is one of several therapy techniques that has been proposed on the BMIT beamline, this method is similar to CT therapy, the difference is that after injecting the contrast agent of high Z into the DNA of the tumor, and irradiate with monochromatic beam with energy above the K-edge of the agent, an auger electron emits. The energy of this electron deposits within the vicinity of their emission to produce photoelectron (photon generated from an element due to ionization). At the ESRF ID17 biomedical beamline, PAT has been applied on male Fisher rat injected with cisdiamminedichloroplatinum (II) (CDDP) platinum contrast agent and irradiated with a high energy monochromatic beam of 78.4 (+/- 0.4) keV. The result showed a high number of auger emission which results in significant enhancement of the effective radiation dose by a factor of two [19, 28].

1.3.2.3 The BMIT–BM

Some of the photon characteristic of the BMIT-BM will make it possible to carry out similar technique as the ID beamline, but some special technique such as KES and absorption imaging will primarily be on the ID beamline. Some methods that use transverse coherent source such as Phase contrast Imaging, X-ray scatter imaging, small angle X-ray scattering and some new technologies would be basically on the BMIT-BM [16, 17].

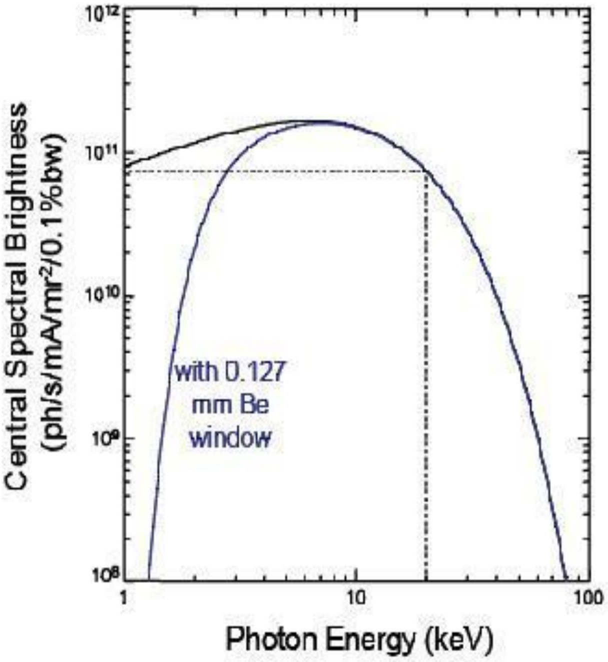

Figure 1.8 Central spectral brightness of CLS bending magnet. The solid blue line shows the brightness with 0.127 *mm Be* window filtration. The dashed line shows 20 *keV* energy [17].

(a) Phase contrast or in-line holography

This is an imaging technique that has been proposed for the bend magnet beamline (BMIT-05BM) at the Canadian Light Source. It uses transversely coherent beam to improve image contrast, this is achieved by the change in phase and amplitude of the incident beam as it transverses the sample [17]. This phase change may then be measured with an interferometer to produce a phase contrast image. Another type of phase contrast called in-line holography will also be examined, with this method; the interference effect produced by the direct and scatted beam causes a change in amplitude of the transmitted beam thereby producing intensity variation in the transmitted beam [19].

(b) X-ray scatters imaging (projection and CT)

This is one of the new imaging techniques that will be carried out on the BMIT-BM beamline. It is similar to computed tomography method, where a pencil beam is used to create an image of a target. The hypothesis is that this technique will be use to distinguish different tissue types with lower exposure [16].

(c) Small angle X-ray scattering

Another scattering imaging technique proposed on the BMIT-BM beamline. This method is described as a potential to be used in both CT and projection imaging with an aim of using the scattering properties of tissues to identify lesions [16].

(d) Development of new imaging technique

An imaging technique that will combine the refraction and extinction contrast mechanisms of DEI/MIR with small angle and wide-angle scattering might be made possible on the BMIT-BM beamline as proposed by Chapman et al.

1.3.2.4 BMIT Detector

For the purpose of biomedical imaging and therapy techniques on the BMIT beamlines, some detectors have been proposed and are presently under review. These detectors are The GE dual energy line detector or the FReLon detector which would be purchased from the ESRF medical beamline, this detector will primary be used for the K-edge subtraction imaging mode, a fluorescence detector system, which is a single element solid state detector and would be used to analyze the imaging beams for the facility and possibly a line beam and area imaging detector which would be used for the DEI, CT, Scatter imaging, and KES techniques [17, 29].

1.3.2.5 BMIT Subject Positioning and Restraint Technology

A fiducial pre-alignment system for positioning wide range of subjects (human and animal with a wide range of sizes and possible projections) and to distinctively mark the region of interest and view outside the experimental hutch before undergoing imaging is been proposed and the bases of this thesis. Also a positioning system, responsible for positioning and scanning large animals and human and that will also position (not scan) small objects is presently under research and development. The positioning range for this system is approx. 3.1 m and the scanning range is about 0.7 m in order to be used for wide imaging scenarios [17]. Other restrain systems that have been proposed are the small- intermediate Animal/Human Sample system for MRT positioning and scanning system and the Large animal positioning and restraint stage, all of which are still under development.

Chapter conclusion:

This chapter gives a survey of some conventional and synchrotron imaging methods use in medical imaging as well as discusses some of the imaging and therapy modalities proposed on the biomedical imaging and therapy beamlines (BMIT) at the Canadian light Source (CLS).

2 Fiducial systems in medical imaging

We will define a fiducial system as a means of pre-alignment of a subject in which a point of beam entry, region of interest and projection are defined on a subject. Medical imaging and therapy methods are based on two major steps. The first step is to determine the location of a target (a specific spot or region on the object) and to determine a projection through the subject. In the case of X-ray radiography, before positioning or alignment to the source, the subject must first be positioned in a view that defines the region of interest and suitable for the type of imaging technique (projection, or CT). The view could be from any of the 3 orthogonal sections of the body (or combinations of) referred to as transverse (separating the body into cranial [superior] and caudal [inferior] parts), median or sagittal (separating the body into left and right parts), and dorsal or frontal (separating the body into dorsal [posterior] and ventral [anterior] parts [31, 32].

In order to get the correct view of the subject and able to align it correctly to the beam, some set out rules must the followed precisely; these are the anatomical, positioning and projection terminologies [31]. These terminologies are use both in conventional and synchrotron imaging methods and they are as follows.

2.1 Anatomical terminology

These terminologies will focus on human and animal subjects in a standard reference position. There are few differences in the anatomic terminologies of human and animal subjects but terms such as dorsal, ventral, cranial, and rostral have the same meaning in the two. Figure 2.1 shows the relationship between the anatomical terminologies use in the both subjects.

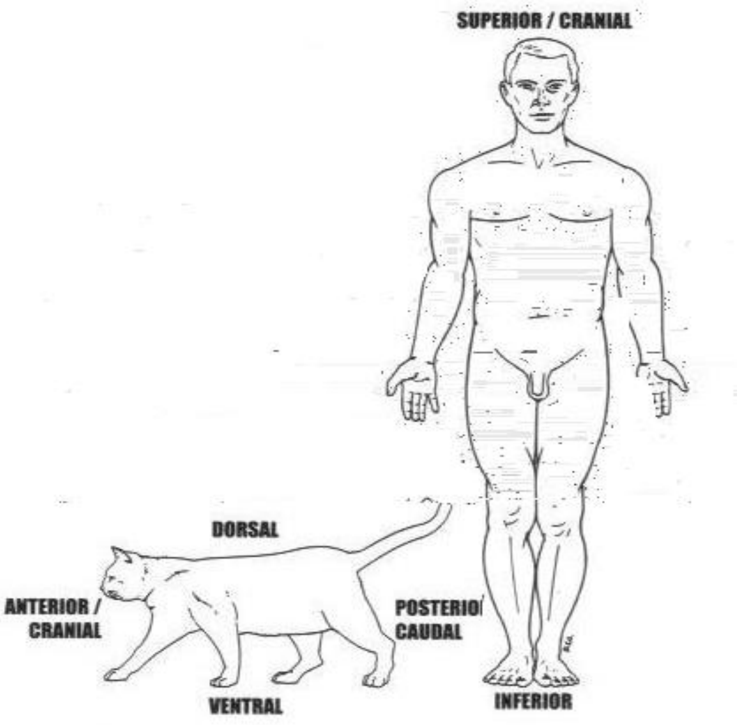

Figure 2.1 Anatomical terminologies in a quadruped and a biped. Figure b shows the quadruped in the synonymous position as the biped [31, 32].

In anatomic view, the subject is erect or stands straight, feet together and arms at sides with palms forward [31, 32]. These views are:

(a) Cranial, cephalic and superior view: View towards the head.

(b) Caudal, caudal and inferior view: View away from the head.

(c) Anterior and Ventral View: front view of the subject.

(d) Posterior or Dorsal View: View from the back of the body or organ of the subject.

(e) Medial or Central View: View to the mid-area or part of the body closest to the midline.

(f) Lateral view: Any view from the side of the subject [32, 33].

2.2 Positioning terminology

Three fundamental planes are used to describe subject positioning in planar and cross-sectional imaging methods, these planes are mutually at right angles to each other [31, 32, 33]. These are:

(a) Median sagittal plane: A vertical plane that runs from front to back and divides the body into right and left portions.

(b) Coronal plane: A plane that runs from side to side and divides the subject or part of the subject into anterior (ventral) to posterior (dorsal) parts.

(c) Transverse or axial plane: A horizontal plane that divides the subject into upper (superior) and lowers (inferior) parts [32, 33]. Figure 2.2 depicts these positioning views as explained above.

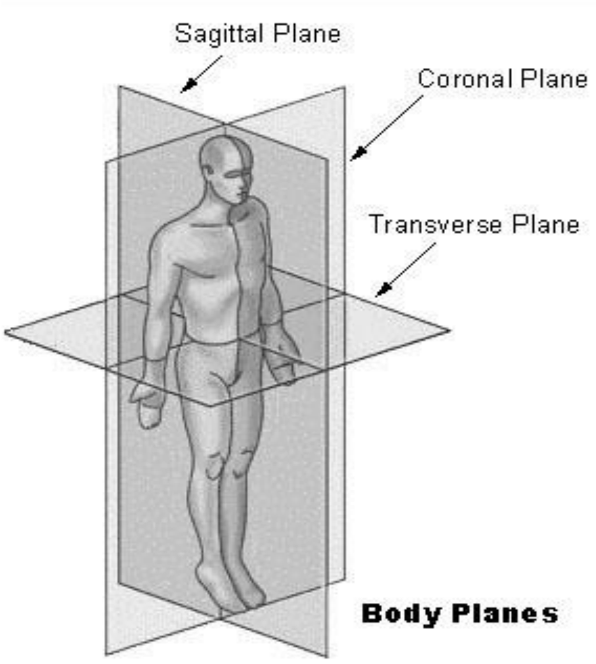

Figure 2.2 Positioning terminologies employ in radiographic imaging [34].

2.2.1 Body positioning terminology

Apart from the three fundamental planes, there are various ways in which subjects could be positioned in relation to the surrounding space [32, 33]. They are:

(a) Erect: In which the projection is taken when the subject is in sitting or standing position.

(b) Recumbent: In this position, the subject is lying down in any of these positions.

(c) Supine (dorsal recumbent) i.e. subject lying on the back.

(d) Prone (ventral recumbent) subject lying face down.

(e) Lateral recumbent subject lying on the side, could be right lateral recumbent- lying on the right side or left lateral recumbent lying on the left side.

(f) Semi-recumbent: subject reclining part way between supine and sitting erect.

2.3 Projection terminology

Projection describes the radiation path as it traverses the subject to the image detector. Different projection terminologies are [31, 32, 33].

(a) Antero-posterior (AP projection): The central ray enters through the anterior (front) aspect, passes along or parallel to the sagittal plane and emerges from the posterior (back) aspect of the subject.

(b) Postero-anterior (PA projection): Here, the central ray is incident on the posterior part, passes parallel to the median sagittal plane, and exits from the posterior aspect of the subject.

(c) Lateral: The central ray passes from one side of the subject to the other side along a coronal and transverse plane. It could be right lateral when the ray enters on the left side and passes through to the detector positioned on the right side, or could be left lateral if the direction of the ray and detector is vice versa.

(d) Oblique: This involves passing the central ray through the subject along a transverse plane at some angle (between zero and 90 degrees) between the sagittal and coronal planes.

(e) Anterior oblique: In this case, the central ray enters through the posterior portion, passes along a transverse plane at some angle to the sagittal plane, and then emerges from the anterior portion.

(f) Posterior oblique: In this projection, the central ray enters the anterior portion; it passes along a transverse plane at some angle to the median sagittal plane, and then emerges from the posterior portion [31, 32, 33].

(g) Lateral oblique: The central ray enters one lateral portion; it passes along a transverse plane at an angle to the coronal plane, and emerges from the opposite lateral aspect [31, 32, 33]. Some projection terminologies are shown in Figure 2.3.

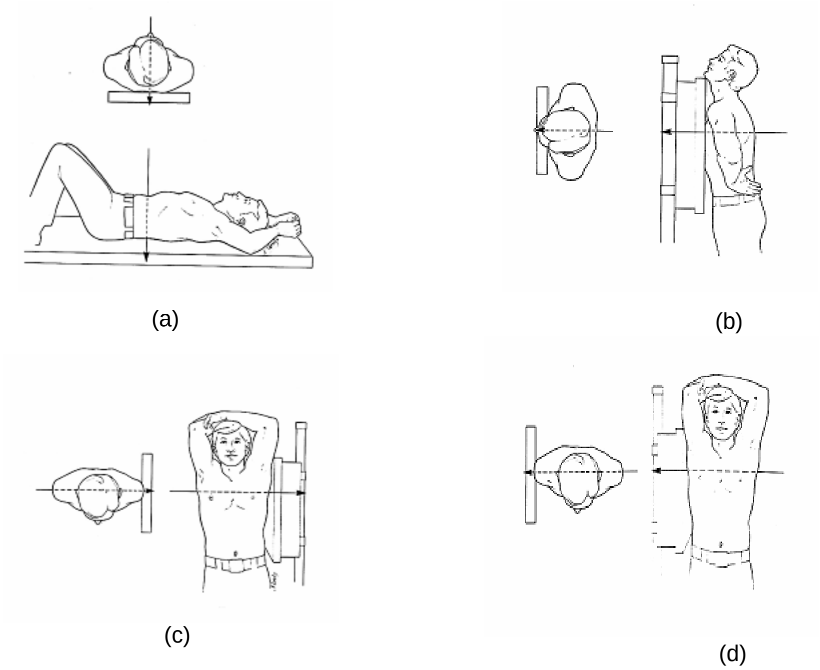

(a) (b)

(c) (d)

Figure 2.3 Shows some projection terminologies (a) AP (Anteroposterior projection), (b). PA (Posteroanterior projection, (c) Left lateral projection,

2.4 Current fiducial system in medical imaging

2.4.1 Invasive Fiducial System

2.4.1.1 Gold Fiducial Marker

An invasive method of stereotactic target localization involves the use of artificial metal fiducial markers which have some property that makes them visible in X-ray images. During treatment planning, these markers are inserted on the target area with the assumption that they would not be misplaced throughout the entire planning and treatment stages. Once these markers are placed, a CT or MRI image is taken to create a reference point for the treatment. With the fiducial still on the target, two different radiography views are then taken during the treatment stage. The images obtained will show the position of the fiducial and then compared with the images acquire during planning. If there is any difference, it is corrected either by manually repositioning the fiducial to the expected area or by aligning the X-ray beam to the exact target location. A typical example of a metal fiducial which has been used is the fiducial gold marker [36]. This marker is cylindrical in shape and manufactured in different sizes and visible in many imaging modalities. This marker is inserted through transrectal ultrasound to the target, and it possesses a feature that makes it remain firmly on the target throughout the entire treatment. Figure 2.4 shows CT and MRI images of prostate cancer using fiducial gold markers [35].

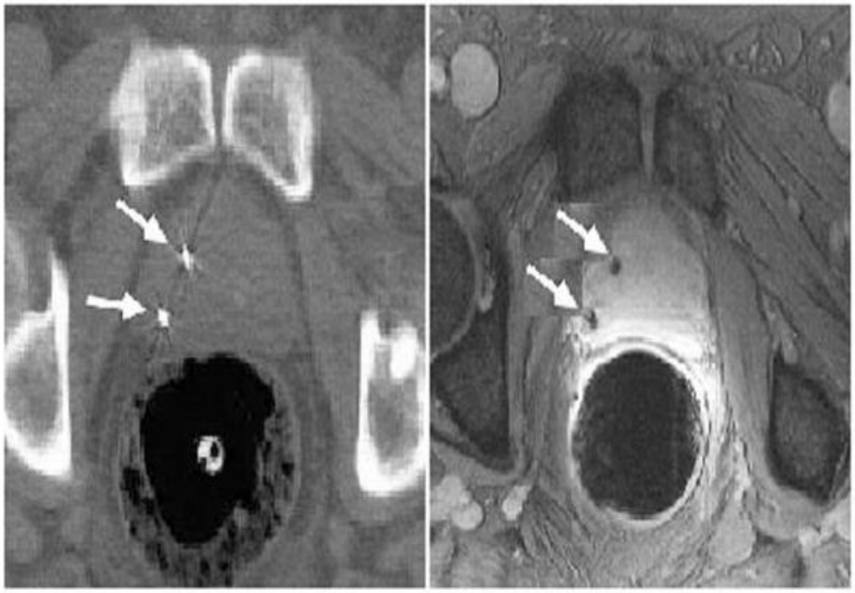

Figure 2.4 Images of a prostate cancer (left) Transverse CT with gold markers shown with the arrows, (right) T2* -weighted MRI with marker also shown with the arrows [35].

2.4.1.2 Carbon Fiducial Marker

Another type of fiducial marker is the carbon fiducial markers described by C. D. Fuller, et al [36]. The only difference between this fiducial and the gold fiducial is that the carbon fiducial is visualisable only in the CT imaging method and therefore not suitable for any other imaging modality. Like the gold metal, it is also administered invasively and the CT image is taken during planning to determine the location of the fiducial on the target. Figure 2.5 shows the comparison between the images acquired using carbon fiducial markers and gold seed fiducial markers [35, 36].

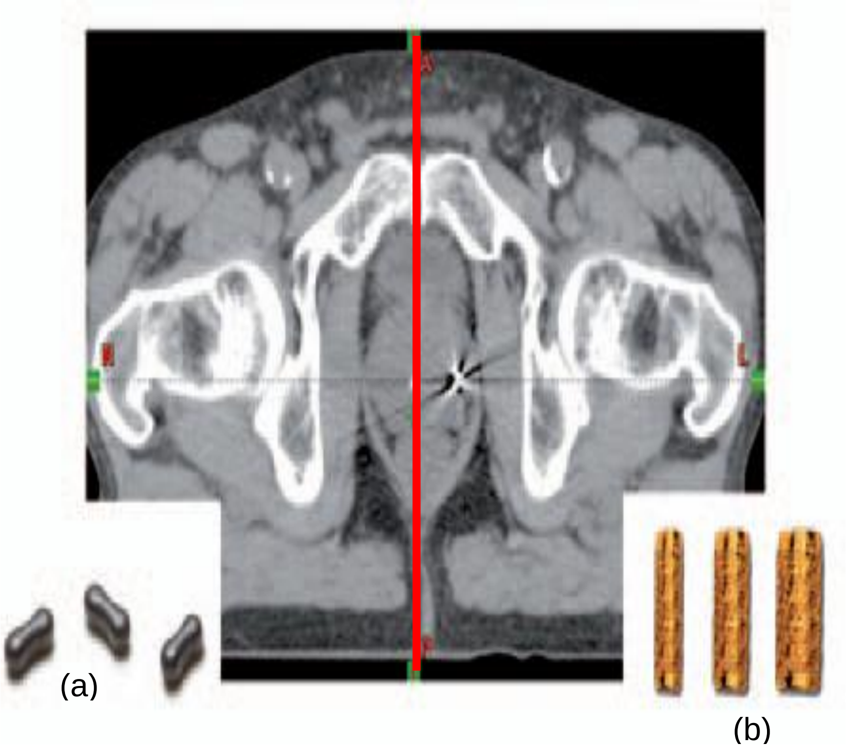

Figure 2.5 Prostrate cancer images showing left (a) transverse CT using Carbon fiducial marker and right (b) with gold fiducial marker [35, 36].

2.4.2 Non Invasive Fiducial System

2.4.2.1 Skull Fiducial Marker System

Both Gold and Carbon fiducial markers are administered invasively to determine target location. Such systems however might not be suitable for some applications which may involve continuous acquisition of multiple volume images, such as producing a radiograph of the brain. A noninvasive, re-attachable skull fiducial marker system was described by Matthew A. Howard III *et al.*, [37] could be used for this repetitive task. This system is made of lightweight re-attachable and movable bars called the Banana Bars that aids the movement of the fiducial marker system to any location on the skull. These bars are firmly connected to the teeth of the subject with the aid of a molded mouth piece which provides a point of attachment for the bars.

Once proper position is established, a CT, MRI and plain X-ray images of the system were taken to show the visibility of the fiducial systems on the radiographs, also to check for any fiducial positioning error which may be corrected before carrying out the treatment [37]. Figure 2.6 below shows the bar and how it was attached to the subject skull and teeth.

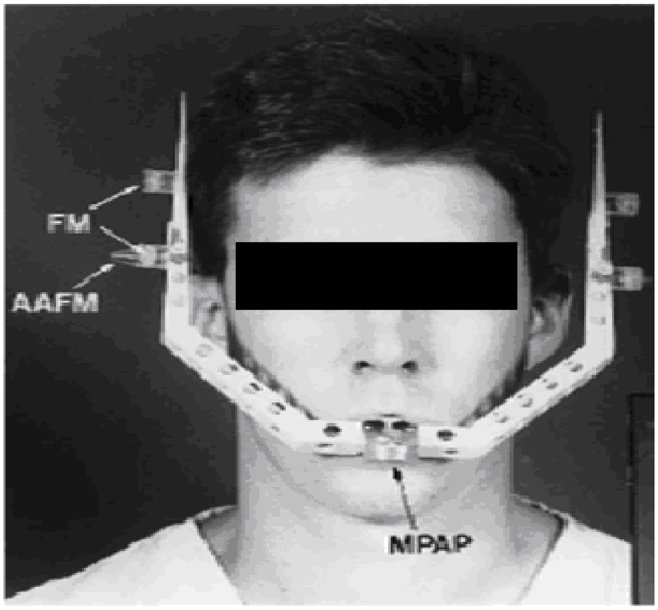
[redacted]

Figure 2.6 A photographic image of the Banana bar mounted on the subject [37].

2.4.3 Stereotaxic Fiducial System

To locate some small deep targets, a clinician sometimes uses a stereotactic head, or frame during treatment planning [3]. This head is rigidly placed over the region of interest, and as usual, a CT or MRI image of the frame is taken to determine the location of the target [1, 3]. However, an internal land mark could also be used instead of the frame to determine this target. A typical stereotactic head is shown below.

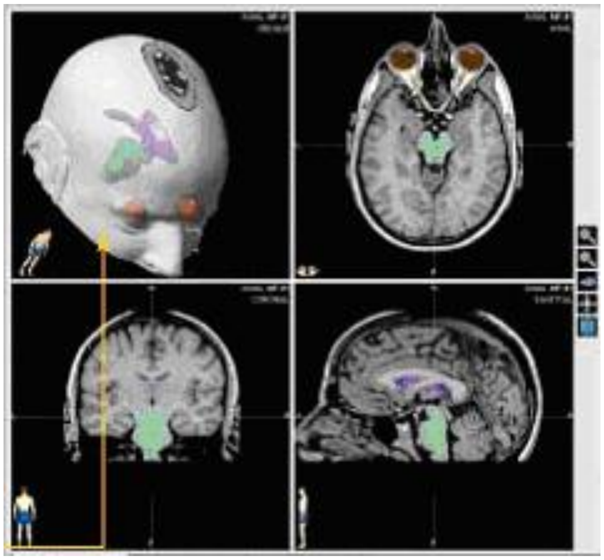

Figure 2.7 MRI scans of the target using a stereotactic head to determine the exact location of the target [3].

During the CT or MRI treatment, this stereotactic head is shown on the scan, which enables the computer to plot the coordinates of the head as well as produce the three-dimensional reconstruction of the target. Other types of noninvasive system are the surgical clips, which are placed at the lumpectomy area during breast imaging [3].

Chapter Conclusion

In this chapter, different fiducial methods, such as invasive and non invasive methods use in medical imaging and therapy were discussed. Some emphases on the current synchrotron fiducial methods and there major disadvantages were also discussed.

3 Fiducial subject pre-alignment system for the biomedical imaging and therapy beamline

The main objective of this chapter is to discuss the proposed fiducial subject pre-alignment system for the BMIT beamlines. The chapter will explain the main objectives of the fiducial system as well as how the goal is achieved.

In synchrotron imaging, the most common system used for subject alignment is based on a laser set placed inside the hutch, which are set to take the same beam path as the X-ray beam. However any method involving subject pre-alignment inside the hutch is very wasteful of the experimental beam time. Therefore, there is a need for an effective and versatile means of positioning wide range of subject outside the hutch.

For this purpose, the design and construction of a prototype fiducial subject pre-alignment system has been proposed for the BMIT beamlines at the CLS. A “fiducial” in this term is a means of pre-alignment in which point of beam entry, region of interest and projection are defined on the subject.

3.1 System Objective

The objective of this fiducial method is to:

(a) Reduce the time it takes to align subject in the biomedical beamlines.

(b) Provide a user friendly way of subject alignment that is more natural to medical community.

(c) Allow mistakes to be corrected before imaging.

This method will allow

(a) Beam path through a specific region of interest to be modeled outside the imaging hutch in a way that it may be reproducible relative to the fixed X-ray beamline inside the hutch.

(b) The model will include an indication of the center of the beam and a rectangular area around the target delineating the limits of the area to be imaged.

(c) The rectangular field of view would be projected on the incoming (entrance) side of the subject as well as the outgoing (exit) side of the subject, and these projections must be coaxial with each other and parallel with the X-ray beam.

To achieve these objectives, two types of positioning systems and a mathematical transformation method will be used:

(a) A C-arm system placed external to the hutch will allow projection to be defined on a specific region of interest on the subject.

(b) A BMIT Kappa style positioning system placed inside the hutch that all subject orientation in position and angle.

(c) A mathematical transformation method that will be used to derive transformation settings from both systems and that will show how the transformation outside the hutch affects transformation inside the hutch.

These positioning systems and the transformations between systems will now be addressed in the next chapter.

4 The C-arm fiducial system, the MRT-Lift and the transformation methods

The positioning system used on BMIT allows subject to be oriented (both in position and angle) relative to the fixed synchrotron radiation beam, as well as allowing a scan of the subject through the beam (translation or rotation). A “C-arm” system external to the hutch will allow projections to be defined using this system; this is more natural for our medical users. The projection information from this C-arm system is used to define the settings of the positioning include both angulations and translation positioning.

4.1 The C-arm Fiducial System

A C-arm fiducial system was designed and constructed using a C-arm machine donated by Saskatoon Health Region. The fiducial system is therefore composed of a C-arm machine, translation stages, and set of laser system. The C-arm system was used to make the incoming rectangular laser beam coaxial with the outgoing beam. Since the system can be rotated about X, Y and Z axes, so co-linearity is achieved by mounting two XY stages on each arm of the machine. On the C-arm, two sets of manually driven XY stages were stacked on each arm of the machine, and on each stage two laser (IIIa classified) system are mounted in a way as to produce a rectangular field of view <20 mm by <30 mm on a pre-marked region of interest on the target. To form this rectangular field of view on a region of interest, two cross lasers are placed side-by-side on a manually driven stage and are made to intercept each other. As these lasers intercept, a rectangular shaped beam is formed. A complete fiducial system designed with solidwork CAD program [41] is as shown in the figures below. The figures show the design of a complete fiducial system, the three axes of rotation of the fiducial machine as well as the formation of the laser beam on a region of interest.

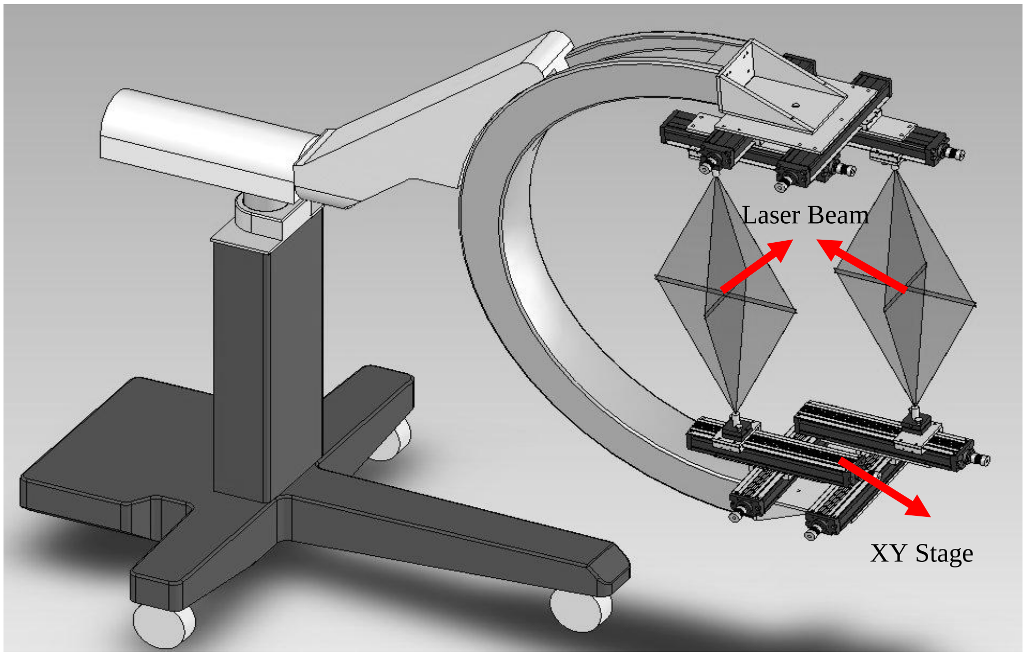

Figure 4.1 Complete solidwork design of the prototype fiducial system

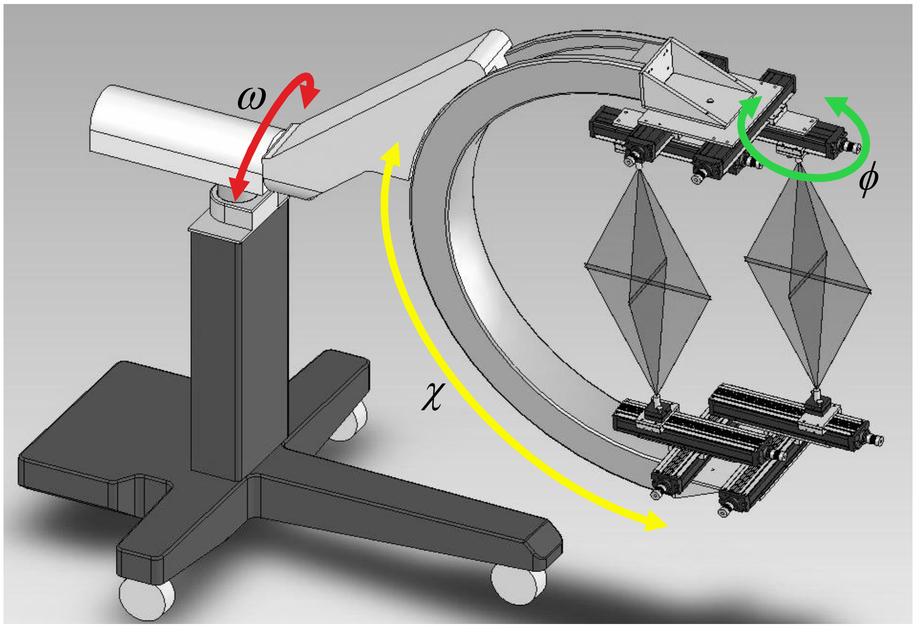

Figure 4.2 Axes of the fiducial

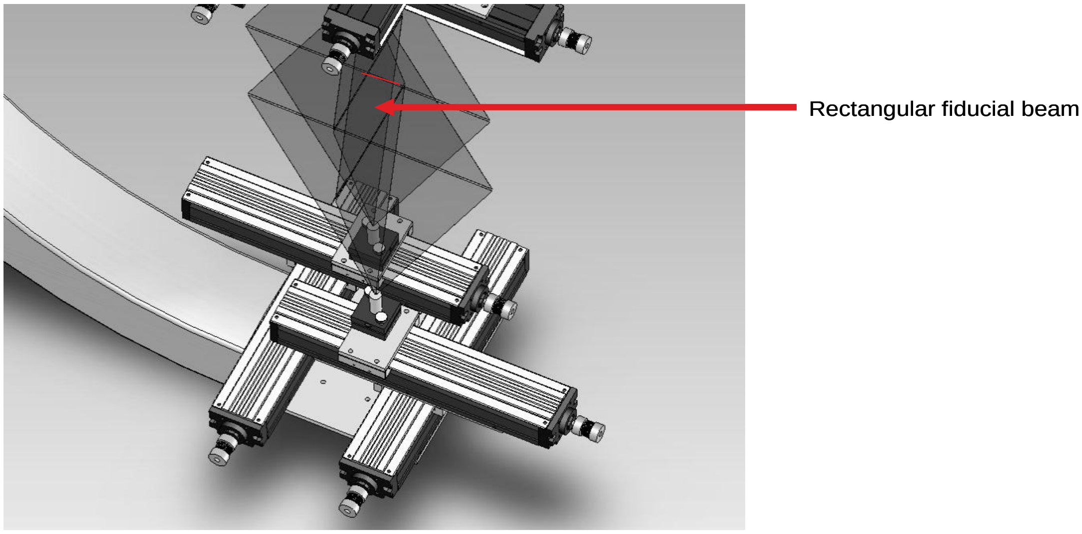

Figure 4.3 A close-up of system arrangement and formation of fiducial beam

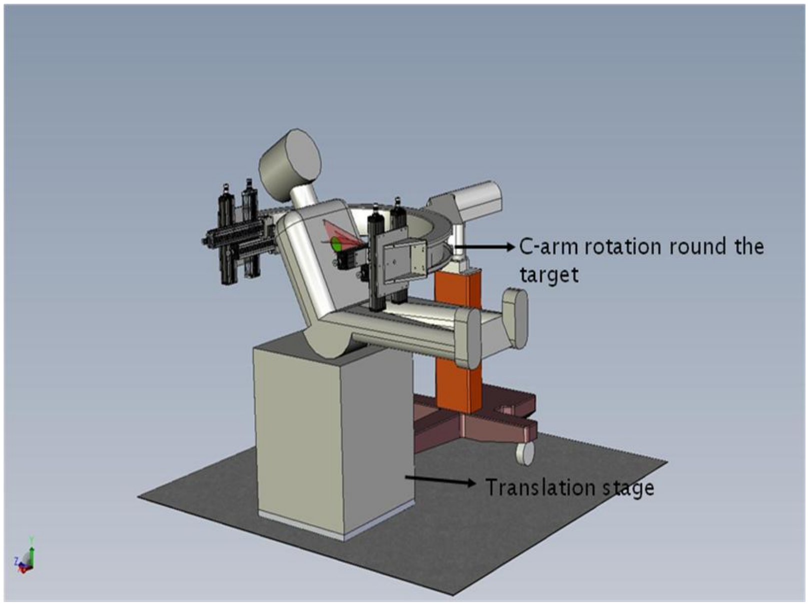

Figure 4.4 Fiducial Laser beam on a region of interest

4.1.1 Fiducial C-arm system construction

A prototype C-arm fiducial system was constructed based on the design criteria. The XY stages and the laser systems were ordered from the manufacturer. The figures below show the XY stages, the assembly and construction of a prototype system.

The C-arm system was used to make the incoming rectangular laser beam coaxial with the outgoing beam by mounting the two XY stages on each arm of the C-arm. As shown in the figure below. The projection information is then stored and analyzed to derive a set of numerical data that was used inside the hutch to reproduce the projection relative to the beamline. Once the two projections are verified, imaging may commence.

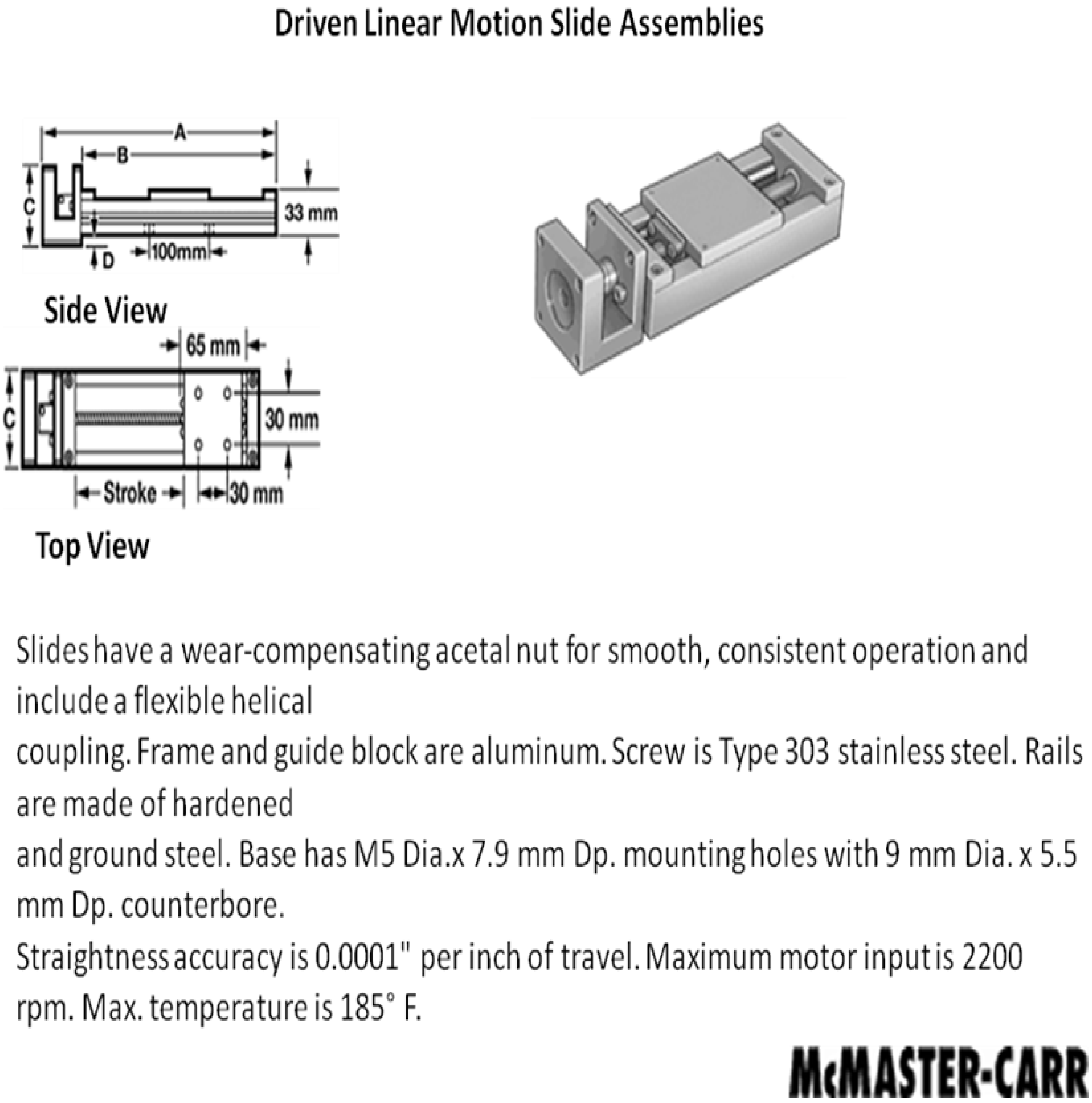

Driven Linear Motion Slide Assemblies

Slides have a wear-compensating acetal nut for smooth, consistent operation and include a flexible helical coupling. Frame and guide block are aluminum. Screw is Type 303 stainless steel. Rails are made of hardened and ground steel. Base has M5 Dia.x 7.9 mm Dp. mounting holes with 9 mm Dia. x 5.5 mm Dp. counterbore. Straightness accuracy is 0.0001" per inch of travel. Maximum motor input is 2200 rpm. Max. temperature is 185° F.

McMASTER-CARR

Figure 4.5 XY translation stage used in construction of the system

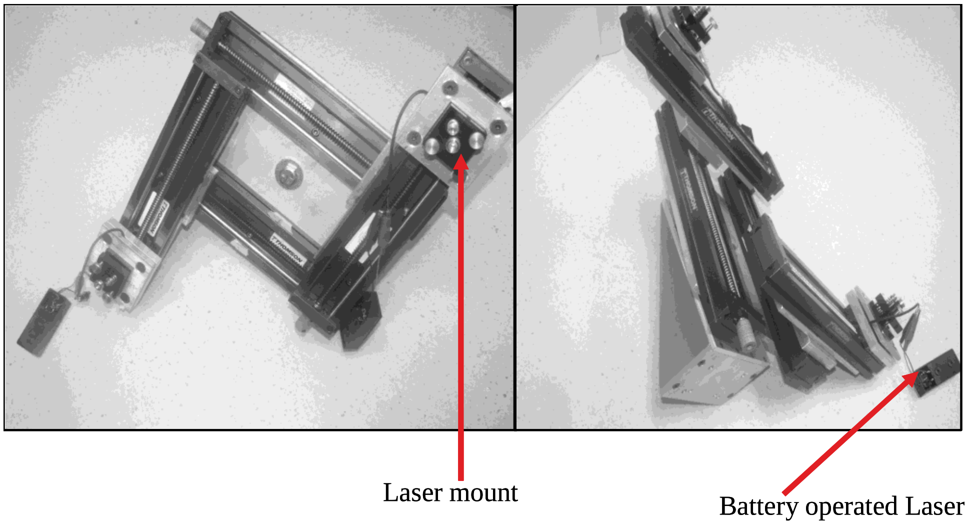

Figure 4.6 Assembling of the XY translation system and the Lasers

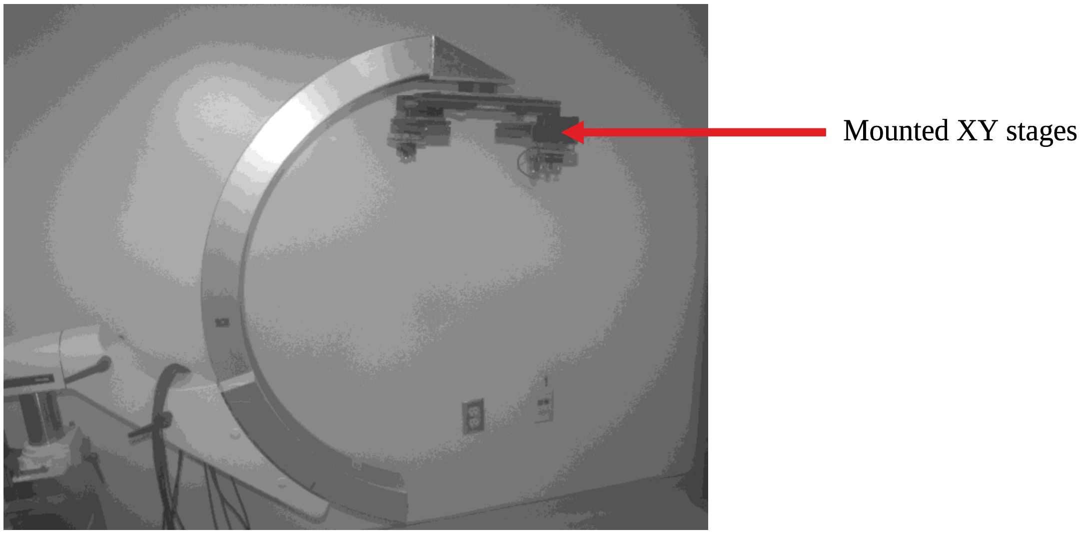

Figure 4.7 Picture of XY translation system as mounted on the C-arm

4.1.2 The C-arm geometry

The C-arm machine uses the same geometry used in single-crystal diffractometer [42]. This geometry is termed the Eulerian. An Eulerian Geometry is the repetition of rotations about a particular axis such as *XYX*, *XZX*, *YXY*, *YZY*, *ZXZ, and ZYZ* [39]. Outside the hutch, the subject to be imaged is placed in a fixed positioning system and the target is positioned relative to the center of the “C” in the C-arm. On the subject, a target is placed with a marker, to indicate the region of interest and where the X-ray beam will hit when placed inside the hutch.

For clarity, the C-arm system is denoted by $\vec{r}^{\,/}$ and the fixed subject by $\vec{r}^{\,//}$.

$\vec{r}^{\,/}$ Is the C-arm frame.

$\vec{r}^{\,//}$ Is the subject frame.

Therefore, it is possible to transform from one frame to another using an appropriate vector rotation, and applying Eulerian method of three successive rotations to transform from subject frame to C-arm frame [43].

Both the fixed C-arm frame and the subject frame have the same origin and they are related by a rotational matrix *F* [42]. The angles of rotation are denoted by ω about x, χ about y, and ϕ about z, such that,

$$\vec{r}^{\,//} = F(\omega,\ \chi,\ \phi)\vec{r}^{\,/}$$ Equation 4.1

For this purpose, the subject is rotated about the *ZXZ* rotation, as shown in the figures below.

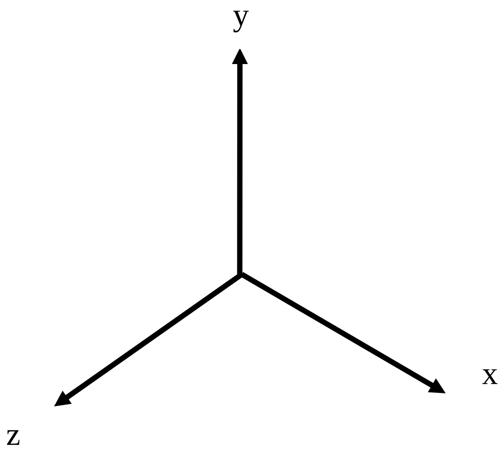

Figure 4.8 The XYZ coordinates of the system.

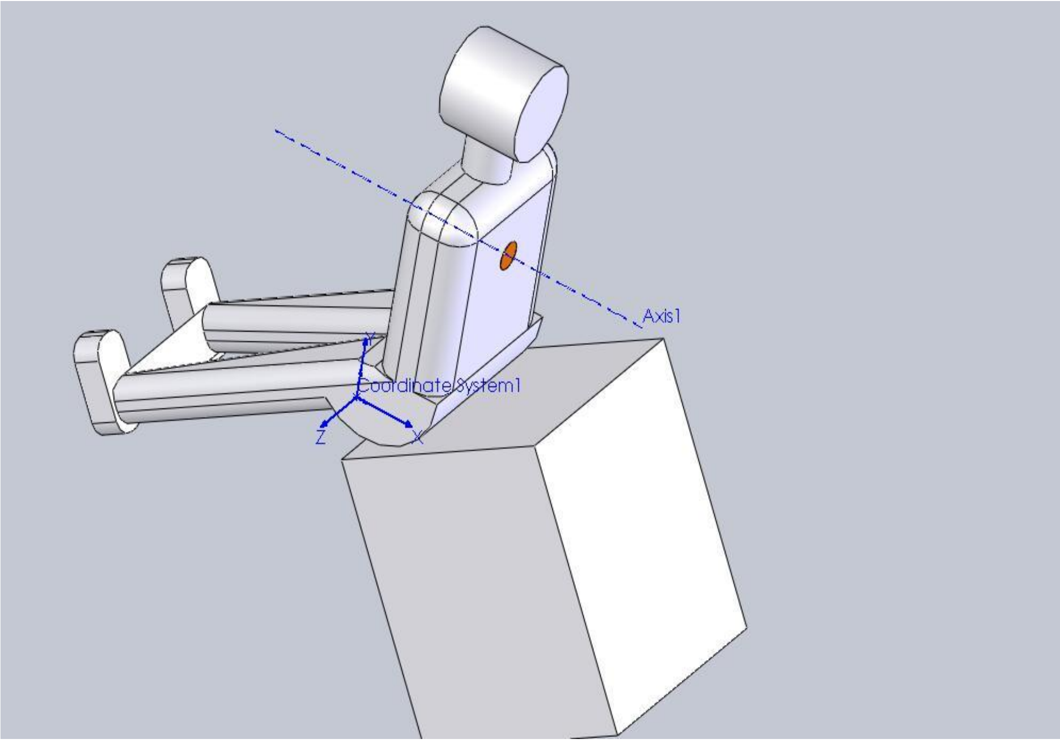

Figure 4.9 The starting view showing the coordinates axis

The first rotation is about the z –axis which is a counterclockwise rotation through angle ϕ as shown below in the figures below.

The coordinates generated through this rotation is $x^{/}$, $y^{/}$ and $z^{/}$.

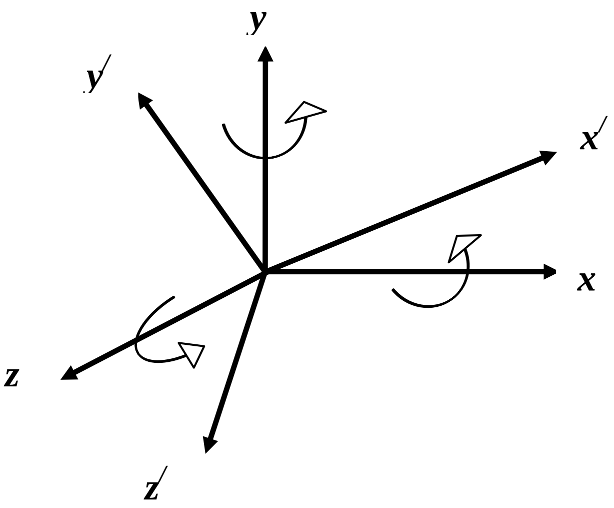

Figure 4.10 Rotation about z- axis about ϕ

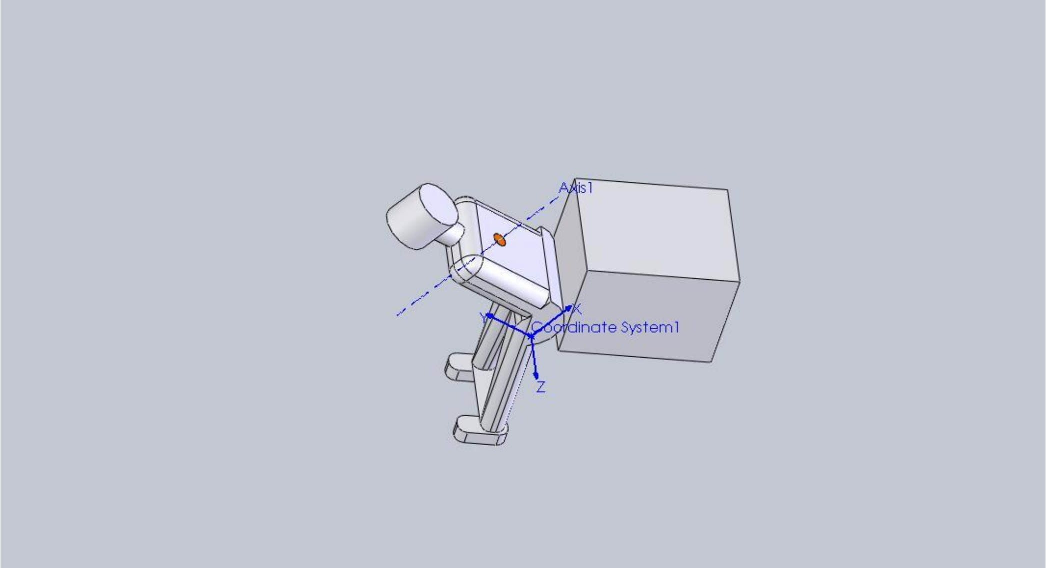

Figure 4.11The view when rotated by z about ϕ

The transformation coordinates is represented as

$$\begin{pmatrix} x^{/} \\ y^{/} \\ z^{/} \end{pmatrix} = \begin{pmatrix} \cos\phi & -\sin\phi & 0 \\ \sin\phi & \cos\phi & 0 \\ 0 & 0 & 1 \end{pmatrix} \begin{pmatrix} x \\ y \\ z \end{pmatrix} \qquad \text{Equation 4.2}$$

The second rotation is through angle ω about $x^{/}$.

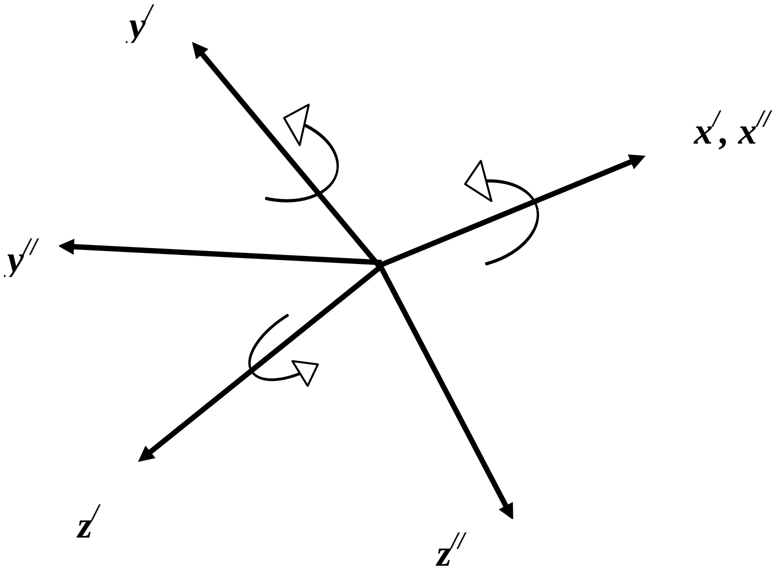

Figure 4.12 Rotation through angle ω about $x^{/}$

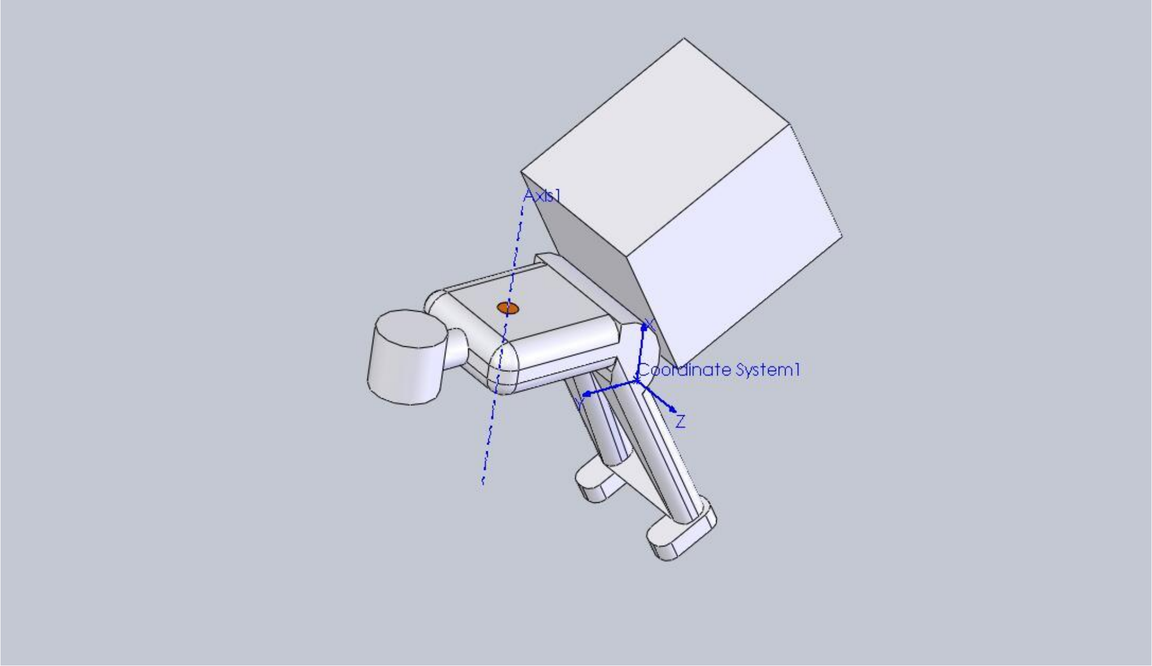

Figure 4.13 Subject view showing rotation through angle ω about $x^{/}$

The transformation of the coordinates is represented as follows:

$$\begin{pmatrix} x^{//} \\ y^{//} \\ z^{//} \end{pmatrix} = \begin{pmatrix} 1 & 0 & 0 \\ 0 & \cos\omega & -\sin\omega \\ 0 & \sin\omega & \cos\omega \end{pmatrix} \begin{pmatrix} x^{/} \\ y^{/} \\ z^{/} \end{pmatrix} \qquad \text{Equation 4.3}$$

The third rotation is about z- axis again though angle χ. The coordinates generated through this rotation is the C-arm frame with coordinates $x^{///}$, $y^{///}$ and $z^{///}$.

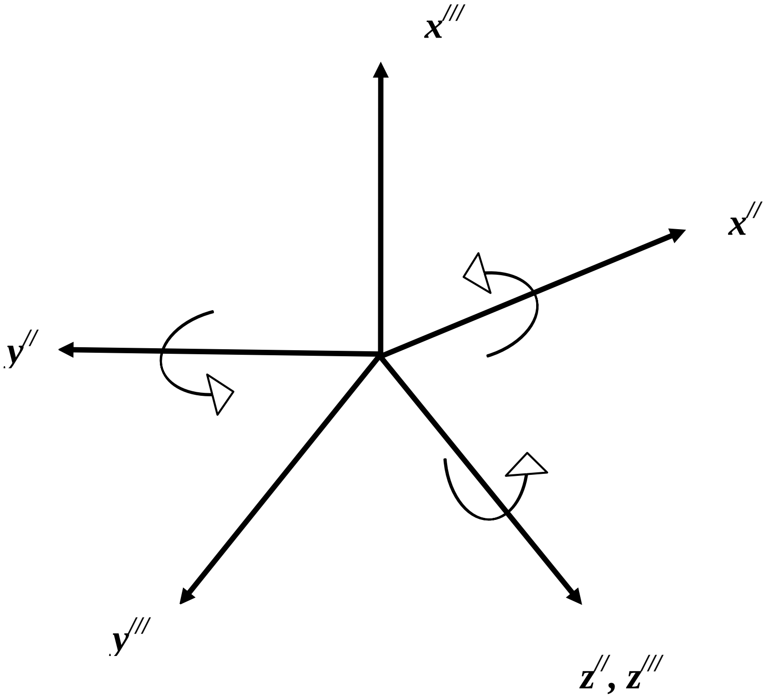

Figure 4.14 Subject rotation through χ about z-axis

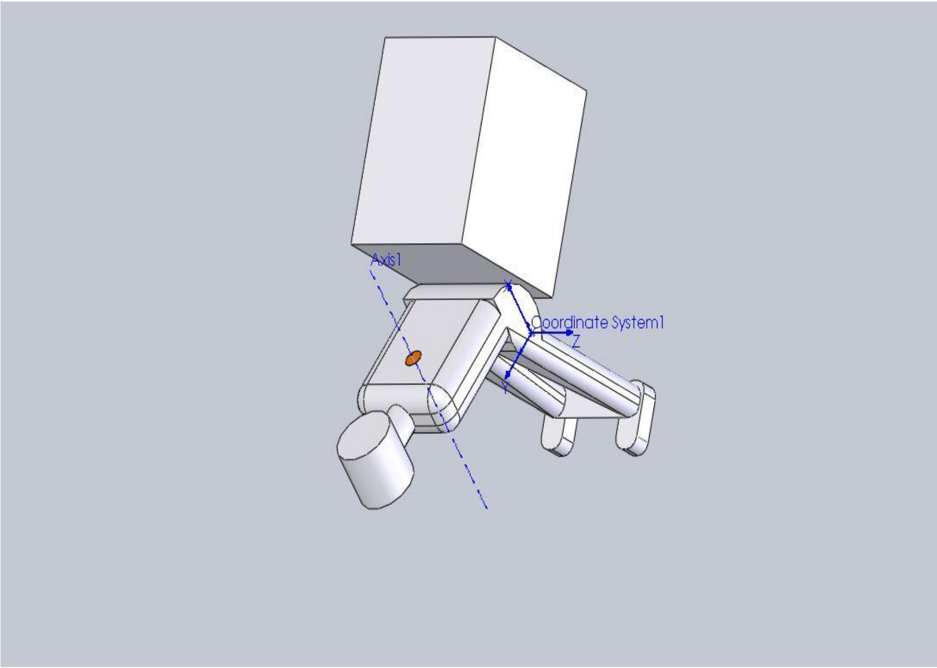

Figure 4.15 Corresponding view of the subject when rotated about χ through z- axis

The transformation coordinates is represented as:

$$\begin{pmatrix} x^{///} \\ y^{///} \\ z^{///} \end{pmatrix} = \begin{pmatrix} \cos\chi & -\sin\chi & 0 \\ \sin\chi & \cos\chi & 0 \\ 0 & 0 & 1 \end{pmatrix} \begin{pmatrix} x^{//} \\ y^{//} \\ z^{//} \end{pmatrix} \qquad \text{Equation 4.4}$$

$$F(\phi,\omega,\chi) = \begin{pmatrix} \cos\phi & -\sin\phi & 0 \\ \sin\phi & \cos\phi & 0 \\ 0 & 0 & 1 \end{pmatrix} \begin{pmatrix} \cos\chi & -\sin\chi & 0 \\ \cos\omega\sin\chi & \cos\omega\cos\chi & -\sin\omega \\ \sin\omega\sin\chi & \sin\omega\cos\chi & \cos\omega \end{pmatrix} \qquad \text{Equation 4.5}$$

$$F(\phi,\omega,\chi) = \begin{pmatrix} \cos\phi\cos\chi - \sin\phi\cos\omega\sin\chi & -\cos\phi\sin\chi - \sin\phi\cos\omega\cos\chi & \sin\omega\sin\phi \\ \cos\chi\sin\phi & -\sin\phi\sin\chi & -\sin\omega\cos\phi \\ \sin\omega\sin\chi & \sin\phi\cos\chi & \cos\omega \end{pmatrix} \qquad \text{Equation 4.6}$$

Equation 4.6 forms a relationship which shows that the C-arm will coincide and form a rectangular shaped beam on the region of interest outside the hutch.

4.2 The MRT-Lift

BMIT will implement a kappa style positioning system whose design is similar (but larger) to that presently use on the ESRF ID17 biomedical beamline [38]. One of the principal applications of this positioning system is for Microbeam Radiation Therapy (MRT) [17]. However; it will be used for imaging (both projection and CT) and therapy methods with subjects as large as humans. The general purpose positioning system is referred to as Microbeam Radiation Therapy Lift (MRTL).

Figure 4.16 shows the design of the MRTL system.

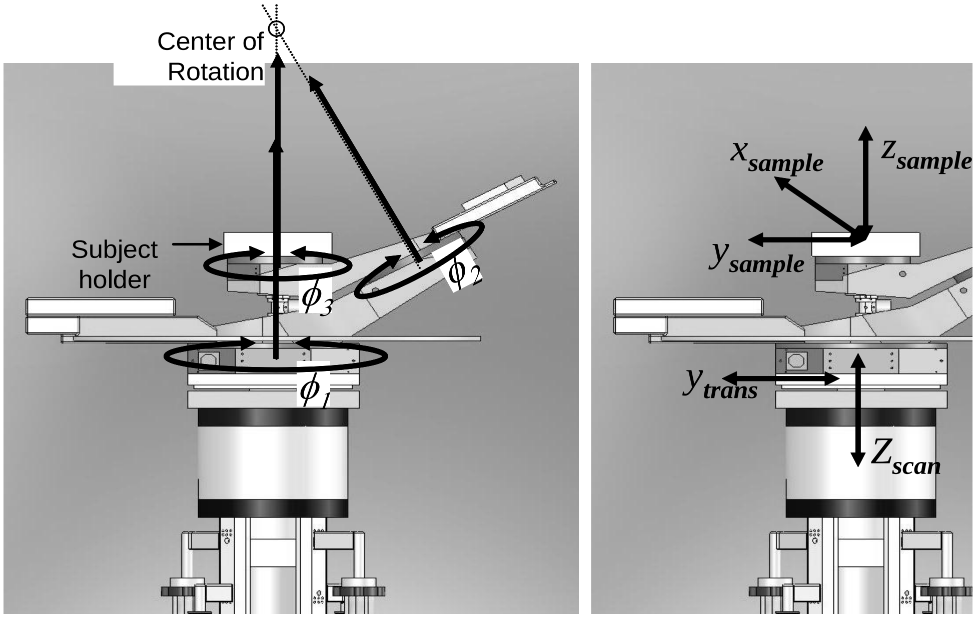

Figure 4.16 MRTL System. Figure (a) shows the rotational axes and figure (b) shows the translational axes.

Where:

Subject holder – Holds the subject in the hutch for imaging.

ϕ_1 Rotates the entire assembly,

ϕ_2 Supports ϕ_3 through angle kappa (30^o) and

ϕ_3 Supports the subject holder

The MRTL system has eight degrees of freedom with three rotational axes and five translations. All the rotational axes intersect at the center of the system (identified as the center of rotation in Figure 4.16 (a). The subject holder is supported on the ϕ_3 axis. Out of the five translational axis, three are located on the subject holder, these are the (x_{sample}, y_{sample}, and z_{sample}) and they are used to locate the subject near to the center of rotation. The ϕ_3 axis is supported by the ϕ_2 axis through a support plate bent by the "kappa" angle. In the MRTL system this angle is 30°. The ϕ_2 axis is supported by another bent plate (also bent by 30°) mounted on the ϕ_1 axis. The ϕ_1 axis rotates the entire assembly of the ϕ_2, ϕ_3 and the sample holder plus the translations (x_{sample}, y_{sample}, and z_{sample}).

Below the ϕ_1 axis is a cross slide (y_{trans}) used to position the center of rotation in the middle of the incident x-ray beam. A vertical translation (z_{scan}) for either positioning or scanning is located below the cross slide.

4.2.1 MRT Coordinate System

For the purposes of this analysis, a coordinate system fixed in the laboratory or attached to the experimental floor is defined as the fixed laboratory frame and the MRTL system is in this frame. The plane perpendicular to the ϕ_1 axis will be denoted as the horizontal plane. The incident X-ray beam is in this plane and the direction defined by this beam is designated as the x-axis[1]. The z-axis is directed upward along the ϕ_1 axis and the y-axis is found using the right-hand rule; shown in Figure 4.17 below.

Figure 4.17 Laboratory based coordinate system for the MRTL system.

The angle of ϕ_2 axis rotation where ϕ_1 and ϕ_3 axes coincide is defined as $\phi_2 = 0$. ϕ_1 is defined to be zero when the cross product of ϕ_1 into ϕ_2 points along the $+y$ direction which places plane of ϕ_1 and ϕ_2 axes in the x-z plane. The last angle ϕ_3 is attached to the subject and is defined by the user. These angles are used to define how the subject is oriented relative to the fixed laboratory frame. Like the C-arm system, the MRTL system is also transformed from the laboratory frame to the subject frame using the matrix transformation method [39]. In this transformation

---

[1] There will be situations where the incident beam may make an angle with respect to the horizontal direction; for example, K-edge imaging. For purposes of clarity, this situation will not be addressed here. This inclined beam will only alter the "projection angle" of the beam though the subject.

techniques, a point in the subject frame is represented by ($\vec{r}_{Subject}$) and the laboratory frame is represented by ($\vec{r}_{Lab}$). When the angles ϕ_1, ϕ_2 and ϕ_3 are altered the frame of the subject is rotated in relation to the fixed laboratory frame. The effect of these three rotations can be calculated by finding the effect of each rotation independently. These are combined to find the effect of all three rotations as shown:

$$\vec{r}_{Lab} = K(\phi_1, \phi_2, \phi_3)\vec{r}_{Subject} \qquad \text{Equation 4.7}$$

Applying a rotational matrix K, such that the rotations about ϕ_1, ϕ_2 and ϕ_3 axes are ϕ_1, ϕ_2 and ϕ_3 degrees. The total effect of the rotation is expressed as:

$$K(\phi_1, \phi_2, \phi_3) = P(\phi_1)O(\phi_2)H(\phi_3) \qquad \text{Equation 4.8}$$

where:

$P(\phi_1)$ is a rotation about the MRT lift ϕ_1 axis by an angle ϕ_1 .

$O(\phi_2)$ is a rotation about the ϕ_2 axis by an angle ϕ_2 .

$H(\phi_3)$ is a rotation about the ϕ_3 axis by an angle ϕ_3 .

The order of the matrix multiplication starts from the axis which directly rotates the subject frame ϕ_3 through the intermediate rotation ϕ_2 and ending with the rotation axis fixed in the laboratory frame ϕ_1. The MRTL positioning has a similar geometry as the four-circle diffractometer geometry (Kappa-geometry) use in X-ray crystallography [39, 40]. Rather than describe the angle convention used in crystallography the kappa equation is modified to suite this purpose.

The Kappa-geometry is defined as:

$$\vec{r}_{Lab} = Z(\omega_K)Y(-\alpha)Z(\kappa)Y(\alpha)Z(\phi_K)\vec{r}_{Sample}$$ Equation 4.9

The modified version for the MRTL geometry is expresses as:

$$\vec{r}_{Lab} = Z(\phi_1)Y(-\gamma)Z(\phi_2)Y(+\gamma)Z(\phi_3)\vec{r}_{Subject}$$ Equation 4.10

Since the MRTL ϕ_2 axis is tilted by γ in the laboratory *X*, *Y* and *Z* system (also shown in Figure 4.17), it is made parallel to the *Z-axis*, by rotating it about Y-axis by angle (γ), and the ϕ_2-axis rotation becomes *Z-axis* rotation. To replace the ϕ_2-axis back to its original position, then we make another rotation about *Y-axis* by (-γ) [40]. Relating the original rotation matrix from Equation 4.8 into the form expressed in Equation 4.9 by making the following assignments:

$$\begin{aligned} P(\phi_1) &= Z(\phi_1), \\ O(\phi_2) &= Y(\gamma)Z(\phi_2), \\ H(\phi_3) &= Y(-\gamma)Z(\phi_3). \end{aligned}$$ Equation 4.11

4.3 Transformation from the C-arm system to MRTL System

The synchrotron X-ray beam is fixed inside the hutch; therefore, there should be a means of aligning the fiducial laser beam formed outside the hutch with the X-ray beam. The object is placed on the MRTL positioning system and it is rotated using set of derived angles to align it with the X-ray beam as will be shown below. The transformation from the C-arm to the MRTL geometry gives two set of matrix equations which are set equal to establish the mathematical relationship between the C-arm angles and the MRTL angles. This results in a set of linear equations which are easily solved as shown below:

To transform C-arm geometry to MRTL geometry, Equation 4.1 and 4.10 are equated [39, 40, 42].

$$Z(\phi_1)Y(-\gamma)Z(\phi_2)Y(+\gamma)Z(\phi_3)\vec{r}_{Subject} = F_Z(\phi)F_X(\omega)F_Z(\omega)\vec{r}_{Subject}$$ Equation 4.12

$$Y(-\gamma)\times Z(\phi_2)\times Y(+\gamma) = Z(\phi-\phi_3)\times X(\omega)\times Z(\chi-\phi_1)$$ Equation 4.13

Substituting *dO* for $(\phi-\phi_3)$ and *dP* for $(\chi-\phi_1)$, then Equation 4.13 becomes

$$Y(-\gamma)Z(\phi_2)Y(+\gamma) = Z(dO)X(\omega)Z(dP)$$ Equation 4.14

$$\begin{pmatrix} \cos(\gamma) & 0 & \sin(\gamma) \\ 0 & 1 & 0 \\ -\sin(\gamma) & 0 & \cos(\gamma) \end{pmatrix} * \begin{pmatrix} \cos(\phi_2) & \sin(\phi_2) & 0 \\ -\sin(\phi_2) & \cos(\phi_2) & 0 \\ 0 & 0 & 1 \end{pmatrix} * \begin{pmatrix} \cos(\gamma) & 0 & -\sin(\gamma) \\ 0 & 1 & 0 \\ \sin(\gamma) & 0 & \cos(\gamma) \end{pmatrix} =$$

Equation 4.15

$$\begin{pmatrix} \cos(dO) & \sin(dO) & 0 \\ -\sin(dO) & \cos(dO) & 0 \\ 0 & 0 & 1 \end{pmatrix} * \begin{pmatrix} 1 & 0 & 0 \\ 0 & \cos(\omega) & \sin(\omega) \\ 0 & -\sin(\omega) & \cos(\omega) \end{pmatrix} * \begin{pmatrix} \cos(dP) & \sin(dP) & 0 \\ -\sin(dP) & \cos(dP) & 0 \\ 0 & 0 & 1 \end{pmatrix}$$

This equals to these nine equations:

$$\cos^2(\gamma)*\cos(\phi_2)+\sin^2(\gamma) = \cos(dO)*\cos(dO)-\sin(dO)*\sin(dP)*\cos(\omega)$$ Equation 4.16

$$\cos(\gamma)*\sin(\phi_2) = \cos(dO)*\sin(dP)+\sin(dO)*\cos(dP)*\cos(\omega)$$ Equation 4.17

$$\sin(\gamma) * \cos(\gamma) * (1 - \cos(\phi_2)) = \sin(dO) * \sin(\omega) \qquad \text{Equation 4.18}$$

$$-\cos(\gamma) * \sin(\phi_2) = -\sin(dO) * \cos(dP) - \cos(dO) * \sin(dP) * \cos(\omega) \qquad \text{Equation 4.19}$$

$$\cos(\phi_2) = -\sin(dO) * \sin(dP) + \cos(dO) * \cos(dP) * \cos(\omega) \qquad \text{Equation 4.20}$$

$$\sin(\gamma) * \sin(\phi_2) = \cos(dO) * \sin(\omega) \qquad \text{Equation 4.21}$$

$$\sin(\gamma) * \cos(\gamma) * (1 - \cos(\phi_2)) = \sin(dP) * \sin(\omega) \qquad \text{Equation 4.22}$$

$$-\sin(\gamma) * \sin(\phi_2) = -\cos(dP) * \sin(\omega) \qquad \text{Equation 4.23}$$

$$\sin(\gamma) * \cos(\phi_2) + \cos^2(\gamma) = \cos(\omega) \qquad \text{Equation 4.24}$$

It follows that Equation 4.18, Equation 4.21, Equation 4.22 and Equation 4.23 show that *dO* and *dP* are equal, so substituted β for both of them, and introducing the half angle for ϕ_2 and ω such that:

$$\cos(\omega) = 2\cos^2(\tfrac{1}{2}\omega) - 1 = 1 - 2\sin^2(\tfrac{1}{2}\omega) \qquad \text{Equation 4.25}$$

$$\sin(\omega) = 2\sin(\tfrac{1}{2}\omega) * \cos(\tfrac{1}{2}\omega) \qquad \text{Equation 4.26}$$

From Equation 4.25 and

Equation 4.26, we derived two sets of equations (normal and alternative) for equations 4.16 through 4.26 [40, 42] Therefore we have:

$$\sin(\gamma) * \sin(\tfrac{1}{2}\phi_2) = \sin(\tfrac{1}{2}\omega) \qquad \text{(N1)}$$

$$\cos(\gamma) * \sin(\tfrac{1}{2}\phi_2) = \sin(\beta) * \cos(\tfrac{1}{2}\omega) \qquad \text{(N2)}$$

$$\cos(\tfrac{1}{2}\phi_2) = \cos(\beta) * \cos(\tfrac{1}{2}\omega) \qquad \text{(N3)}$$

The alternative solutions are:

$$\sin(\gamma) * \sin(\tfrac{1}{2}\phi_2) = -\sin(\tfrac{1}{2}\omega) \qquad \text{(A1)}$$

$$\cos(\gamma) * \sin(\tfrac{1}{2}\phi_2) = -\sin(\beta) * \cos(\tfrac{1}{2}\omega) \qquad \text{(A2)}$$

$$\cos(\tfrac{1}{2}\phi_2) = -\cos(\beta) * \cos(\tfrac{1}{2}\omega) \qquad \text{(A3)}$$

In the normal equation, one to one relation exists between ϕ_2 and ω such that ω covers the range $-60^o \le \omega \le +60^o$ while ϕ_2 covers the range $-180^o \le \phi_2 \le +180^o$. Thus equation N1 becomes:

$$\sin(\tfrac{1}{2}\phi_2) = \frac{\sin(\tfrac{1}{2}\omega)}{\sin(\gamma)} \qquad \text{Equation 4.27}$$

$$\cos(\tfrac{1}{2}\phi_2) = \frac{(\sin^2(\gamma) - \sin^2(\tfrac{1}{2}\omega))^{\frac{1}{2}}}{\sin(\gamma)} \qquad \text{Equation 4.28}$$

Substituting $\sin(\tfrac{1}{2}\phi_2)$ in (N2) and (N3)

$$\sin(\beta) = \frac{\cos(\gamma) * \sin(\tfrac{1}{2}\omega)}{\sin(\gamma) * \cos(\tfrac{1}{2}\omega)} \qquad \text{Equation 4.29}$$

$$\cos(\beta) = \frac{(\sin 2(\gamma) - \sin 2(\tfrac{1}{2}\omega))^{\frac{1}{2}}}{(\sin(\gamma) * \cos(\tfrac{1}{2}\omega))} \qquad \text{Equation 4.30}$$

Equations 4.27 through 4.29 are used to derive the angular values that are used in both systems for the transformation. The derived values are shown in chapter 5 in Table 5.1.

Chapter Conclusion

This chapter started by explaining the Eulerian geometry method use in matrix transformation, it explains and shows the mathematical derivatives used to transform the C-arm fiducial system from one frame to another, as well as the transformation of the laboratory frame MRTL system to the subject frame. The chapter is concluded by showing the transformation from outside the hutch to inside the hutch using the kappa geometry method to generate set of equations that are used to derive angular values for both systems.

5 Simulation Results

Solidworks CAD program [41] was used for the system design and testing. Figure 4.1 shows the complete design of the system while appendix A-D shows the detailed drawing of the system. All the possible angles of the fiducial C-arm system and the MRTL system were analyzed using the CAD program. The results show the combined equations that produce the transformation from outside the hutch to the target on the MRTL system inside the hutch. The system was tested by first setting all of its angles to zero (using the initial laser alignment procedure outline in appendix A, and focusing it on a flat surface as shown in Figure 5.1**Error! Reference source not found.**. The maximum measured dimension of the projected beam was estimated to be about $20\ cm \times 30\ cm$, neglecting beam divergence.

After a desired dimension is achieved, a subject (dog) with a targeted region of interest was mounted on a flat platform which acts as a positioning table and the beam is projected on the target, so as to produce the same rectangular laser beam, as shown in Figure 5.2. Several angles of the fiducial system and the MRTL system which were derived from the transformation equations are as shown in Table 5.1. These angles were used to transform from outside the hutch to inside the hutch.

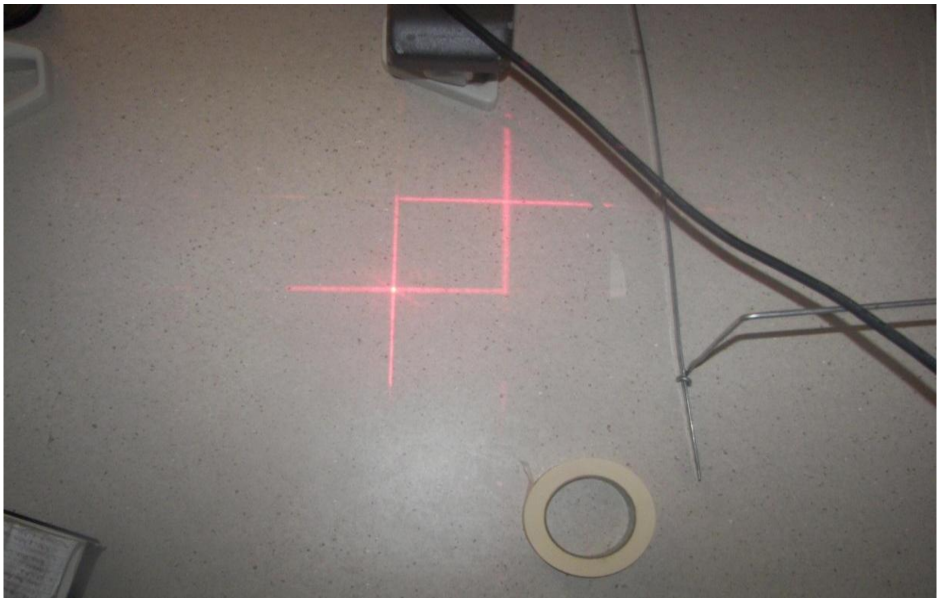

Figure 5.1 Rectangular laser beam formed on a flat surface

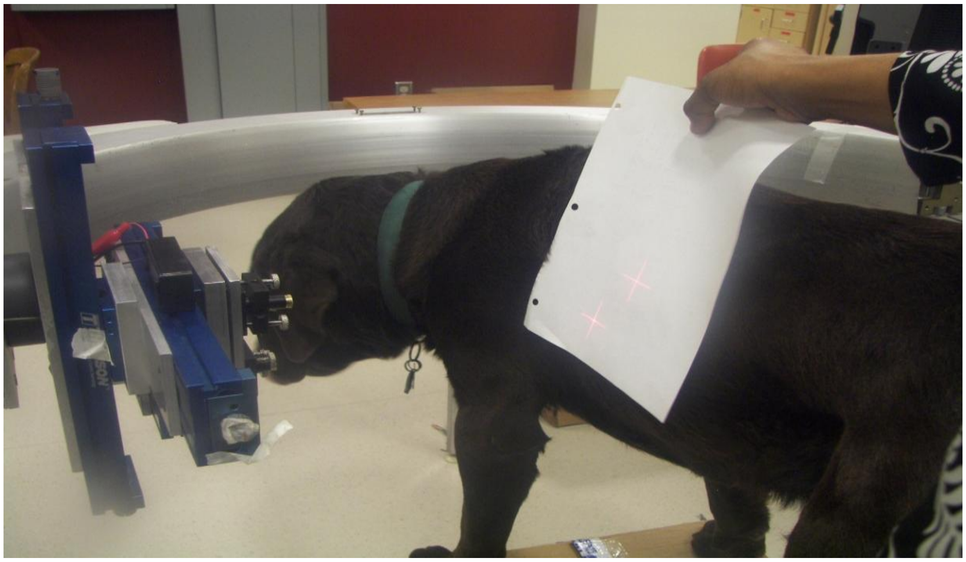

Figure 5.2 Formation of a rectangular beam on a subject

Fiducial System Values			MRTL Values		
ω	χ	ϕ	ϕ_1	ϕ_2	ϕ_3
0.00	0.00	0.00	90.00	0	90.00
30.00	0.00	0.00	30.00	40.21	90.00
60.00	0.00	0.00	0.00	180.00	0.00
0.00	30.00	0.00	90.00	0.00	120.00
0.00	60.00	0.00	90.00	0.00	150.00
0.00	0.00	30.00	90.00	0.00	90.00
0.00	0.00	60.00	90.00	0.00	90.00

Table 5.1 List of possible angular settings for the Fiducial and the MRTL systems

5.1 Result Analysis from Table 5.1

(1) Based on the values from Table 5.1 above, and starting with the first row where the values, of the C-arm fiducial systems are $\omega = 0^o, \chi = 0^o \; and \; \phi = 0^o$ and the values of the MRTL system are $\phi_1 = \phi_3 = 90^o, \phi_2 = 0^o$ then figures 5.3 and 5.4 below indicate the transformation that takes place and how the beam hits the target at the same position both inside and outside the hutch.

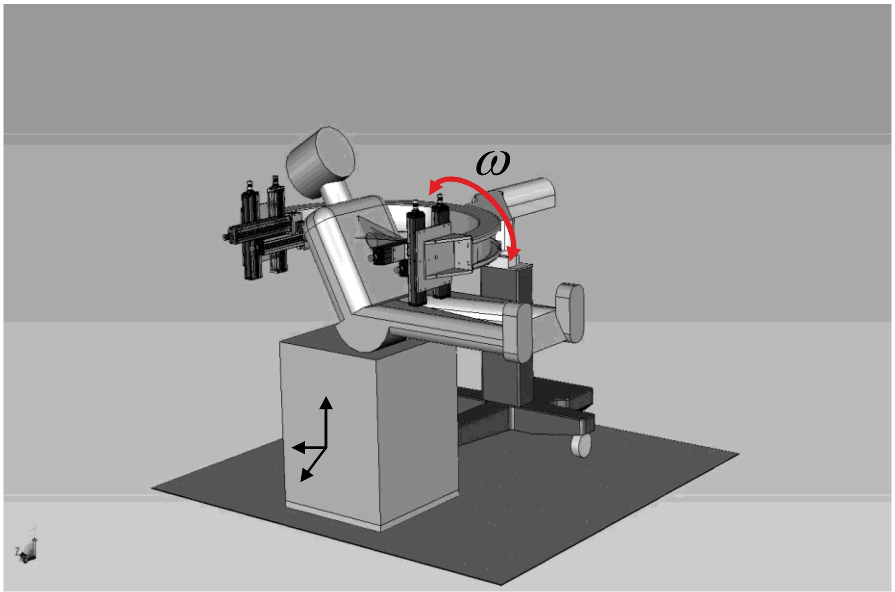

Figure 5.3 Initial settings of the fiducial system at ω =0, χ =0, and ϕ =0

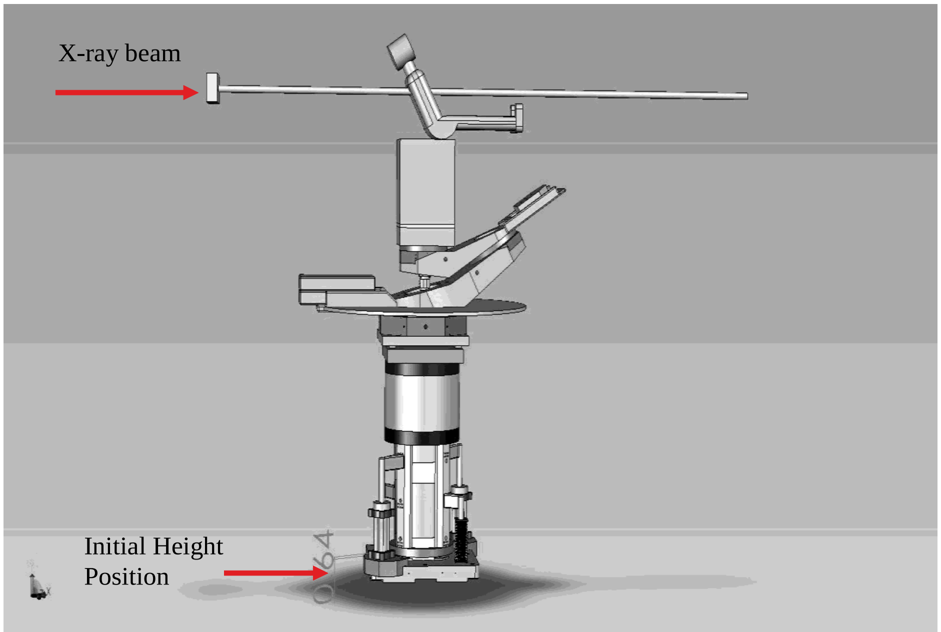

Figure 5.4 Initial settings of the MRTL system at $\phi_3 = \phi_1$ =90, ϕ_2 =0

(2) Another example is row three of the Table 5.1, where values of the fiducial system are $\omega = 60^o, \chi = 0^o \ and \phi = 0^o$ and values of the MRTL system are $\phi_1 = \phi_3 = 0, \phi_2 = 180^o$.

Figures 5.5 and 5.6 indicate the transformations that happen between the systems.

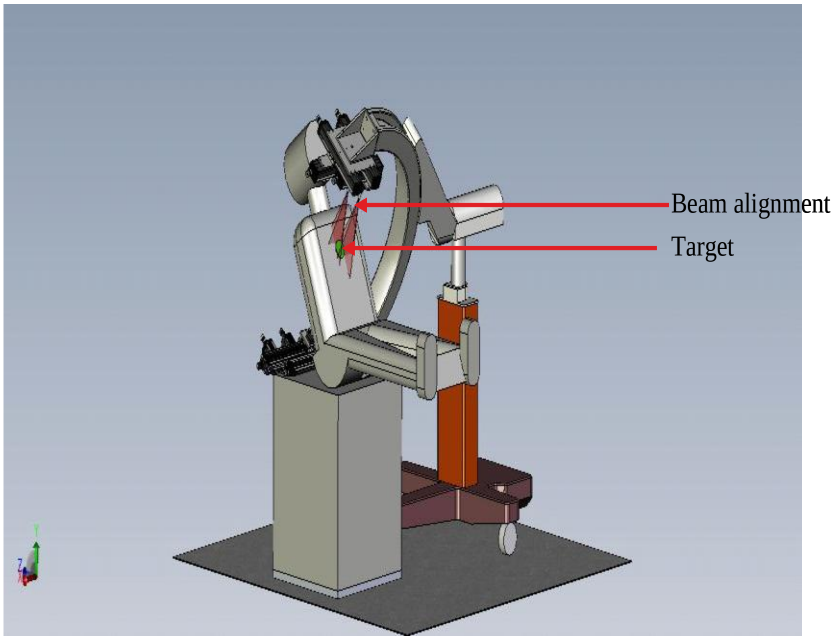

Figure 5.5 Setting of the fiducial system at $\omega = 60^o, \chi = 0^o \; and \phi = 0^o$ outside

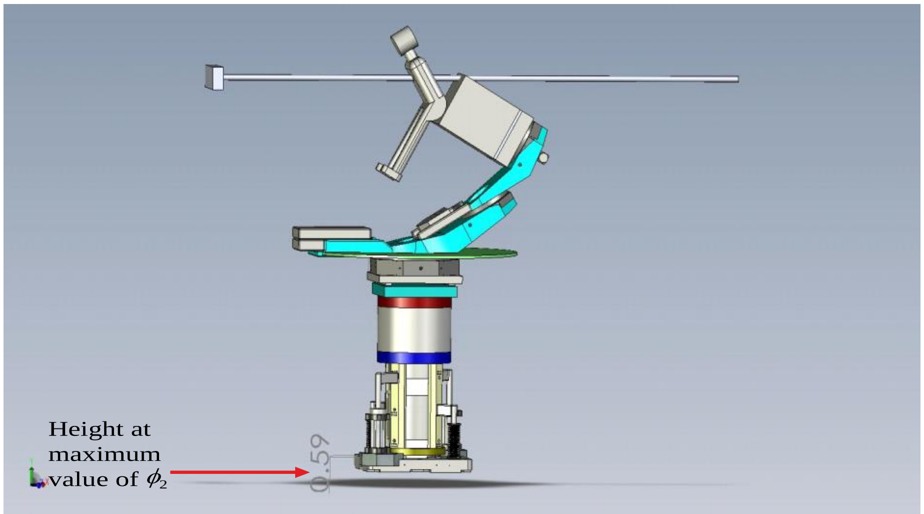

Figure 5.6 Corresponding setting of the MRTL angles ($\phi_1 = \phi_3 = 0, \phi_2 = 180^o$) inside the hutch

5.2 Design Limitation

Design and construction limitations are usually associated with all electromechanical systems. Some of the verified limitations of the fiducial system are discussed below:

(a) Omega axis angle (ω) can only be rotated within the range of $-60^o \le \omega \le +60^o$ this is due to the angular limitation of 30 degree of the MRTL angle. If it exceeds this range the laser will be out of range and alignment will not be possible.

(b) The ϕ_2 angle of the MRTL system can also cover the range $-180^o \le \phi_2 \le +180^o$ so as to keep the object in a safe position.

(c) Not all calculated values of the angles were able to align both systems (fiducial and MRTL system) to the region of interest, but the values used to align the system are as tabulated in Table 5.1.

This system has however not been used for any particular synchrotron imaging method, and has not also been tested on small lab animals such as (Lab rats) but it may be used on any size of subject, provided its dimension and angles are adjusted to suite the purpose.

Chapter Conclusion

In this chapter, the results obtained from the two systems have been demonstrated. The results indicate the validity of the mathematical methods, as well as the design approach. It gives the demonstrations of some of the values taken from the transformation table and how the systems were able to transform from outside the hutch to inside the hutch. It also shown some of the design limitation of the two systems.

6 Conclusion and future work

6.1 Conclusion

In this thesis, the non-invasive and invasive fiducial method use in conventional and synchrotron imaging modalities were analyzed. The main focus was on the fiducial imaging method designed for the biomedical imaging and therapy beamlines at the Canadian Light Source.

In synchrotron imaging, there is no specific system for subject pre-alignment before imaging or therapy, and some of the systems use for this purpose, require positioning the subject inside the imaging hutch, which makes such systems wasteful of experimental beam time. However, this work has been able to demonstrate a method of pre-alignment in subject (e.g., human, animal specimen) in a location remote from an imaging light source using a similar kappa geometry method to establish the relationship between the C-arm fiducial subject pre-alignment system and a MRTL positioning system.

The fiducial pre-alignment method is made up of a C-arm fiducial pre-alignment system, a BMIT kappa style positioning system and a mathematical transformation method, which aid in transforming from one system to another. The system has shown the capability of transferring a 3-dimensional data from outside to inside synchrotron imaging experimental hutch with high fidelity, thus preserving valuable beam time. The system will:

(a) Reduce the time it takes to align subject in the biomedical beamlines.

(b) Provide a user friendly way of subject alignment that is more natural to medical community.

(c) Allow mistakes to be corrected before imaging

6.2 Future Work

The scope of this thesis is to design and construct a prototype fiducial system. However for further research and system implementation, these suggestions should be taken into consideration:

1. Finish the c-arm laser system construction. Outstanding tasks include:
    a. Make second laser system on opposite side.
    b. Motorize the stages.
    c. Develop software / joystick driven system to allow easy manipulation of region of interest.
2. Encode c-arm axes.
3. Input encoded angles into computer 3-dimensional model of c-arm and Huber.
4. Establish limits of motion, i.e. alarm when limit of motion of MRTL is reached.
5. Use a true bidirectional stages instead of stacking two unidirectional stages.

The present prototype shows the promises of reducing imaging time at most synchrotron facility but the system could not be tested on any beamline because the intended beamlines (BMIT Beamlines) have not been completed as at the time of this thesis, so there was no further way to verify our hypothesis but to rely on the design and mathematical analysis.

7 References

1. Erdi YE, Wessels BW, DeJager R, Erdi AK, Der L, Cheek Y, Shiri R, Yorke E, Altemus R, Varma V, Smith LE, Hanna MG. **A New Fiducial Alignment System to Overlay Computed Tomography or Magnetic Resonance Anatomical Images with Radio-labeled Antibody Single –Photon Emission Computed Tomographic Scans.** Cancer. 1994; **73**:923-931.
2. Simon DA. **What is "Registration" and Why is it so Important in CAOS.** First Joint CVRMed / MRCAS Conference. 1997; 57-60.
3. Breneman J, Warnick R. **Introduction to Radiation Therapy.** Precision Radiotherapy. 2003; 1-6.
4. Bayat S, Le duc G, Porra L, Berruyer G, Nemoz C, Monfraix S, Fiedler S, Thomlinson W, Suortti P, Standertskj¨old-Nordenstam CG, Sovij¨arv ARA. **Quantitative Functional Lung Imaging with Synchrotron Radiation using Inhaled Xenon as Contrast Agent .** Phys. Med. Biol **.** 2001; **46**:3287-3299.
5. Hendee WR, Ritenour ER. **Medical Imaging Physics**: 4th ed. Wiley-Liss, Inc., New York. 2002; 2-7
6. Sprawls P. **The Physical Principles of Diagnostic Radiology**. University Park Press.1977; 1-31.
7. Meredith WJ. **Fundamental Physics of Radiology**: 3rd ed. John Wright & Sons Ltd. 1977; 44-79.
8. Cherry P, Duxbury A. **Practical Radiotherapy Physics and Equipment**: London Greenwich Medical Media. 1998; 21-49.
9. Momose A, Takeda T, Yoneyama A, Koyama I, Itai Y. **Phase-Contrast X-Ray Imaging Using an X-Ray Interferometer for Biological Imaging.** Analytical Sciences. 2001; 116-117.
10. Guy C. **An Introduction to the Principles of Medical Imaging**. London Imperial College Press. 2005; 169-300.
11. Lewis RA, Yagi N, Kitchen MJ, Morgan MJ, Paganin D, Siu, KKW, Pavlov K, Williams I, Uesugi K, Wallace MJ, Hall CJ, Whitley J, Hooper SB. **Dynamic Imaging of the Lungs Using X-ray Phase Contrast.** Phys. Med. Biol. 2005; **50:**5031-5040.
12. Bushberg JT, Siebert JA, Leidholdt EM, Boone JM. **The Essential Physics of Medical**

Imaging: 2nd ed. Lippincott Williams & Wilkins. 2002; 415-548.

13. Henderson GS, Baker DR. **Synchrotron Radiation: Earth, Environmental and Material Sciences Applications**: Mineralogical Association of Canada. 2002; 56-120.
14. Chao A, Moser HO, Zhao Z. **Accelerator Physics, Technology and Applications, selected lectures of OCPA International Accelerator School**. World Scientific. 2004; 500-627.
15. Matthew Dalzell. **Canadian Light Source Activity Report 2001 - 2004.** Canadian Light Source. 2005; CLS Document Number 0.18.1.2.
16. Chapman D. **Biomedical Imaging and Therapy Beamline Preliminary Design Report.** Canadian Light Source. 2006; CLS Document Number. 26.2.1.2.
17. Chapman D. **BioMedical Imaging and Therapy Beamline Conceptual Design Report**. Canadian Light Source. 2006; CLS Design Note 26.2.1.1.
18. Chapman D. Private Communication, March 17th 2006.
19. Suortti P, Thomlinson W. **Medical Applications of Synchrotron Radiation.** Institute of Physics Publishing. 2003; **48**:1-35.
20. Richardson, J.M.; Petr, R.; Theophanis, S.; Chapman, LD. **Dual-energy digital subtraction angiography using characteristic radiation and K-edge filtration**. IEEE. 1996; **3**:1545 – 1546.
21. Yamashita T, Kawashima S, Ozaki M, Namiki M, Hirase T, Inoue N, Hirata K, Umetani K, Sugimura K, Tokoyama M. **Mouse Coronary Angiography Using Synchrotron Radiation Micro-angiography.** Circulation. 2000; 105:3-4**.**
22. Casteele EVd, Dyck DV, Sijbers J, Raman E. **An Energy–based Beam Hardening Model in Tomography.** Phys. Med. Biol**.** 2002; **47:**4181-4190.
23. Hasnah MO, Zhong Z, Oltulu O, Pisano ED, Johnson RE, Sayerd D, Thomlinson W, Chapman D. **Diffraction Enhanced Imaging Contrast Mechanism in Breast Cancer Specimen** . Med Phys. 2002; **29:**2216-21.
24. Lewis R. **Medical Applications of Synchrotron Radiation X-rays** 1997 Phys. Med. Biol. 1997; **42:**1213-1243.
25. Thomlinson W, Suortti P, Chapman D: **Recent Advances in Synchrotron Radiation Medical Research.** Nuclear Instruments and Methods in Physics Research Section A. 2005; **543**: 288-296.

26 Muehleman C, Li J, Zhong Z, Brankov JG, Wernick MN. **Multiple-image Radiography for Human Soft Tissue.** Journal of anatomy. 2006; **208:**115-124.

27. Laissue JA, Blattmann H, Wagner HP, Grotzer MA, Slatkin DN. **Prospects for Microbeam Radiation Therapy of Brain Tumours in Children to Reduce Neurological Sequelae**. Dev Med Child Neurol. 2007; **49**:577-81.
28. Humm J. **Therapy by Photon Activation.** PubMed Nature. 1988; **336**:710-1
29. Nagarkar VV, Shestakova I, Gaysinskiy V, Tipnis S.V, Singh B, Barber W, Hasegawa B, Entine G. **A CCD-based detector for SPEC**. IEEE. 2004; **4:**2449 – 2452.
30. Christensen CR, Adams GP. The **Biomedical Imaging and Therapy Research Beamline at the Canadian Light Source.** Can. Vet. Journal. 2003; **44**:966–967.
31. Eisenberg RL, Dennis CA, May CR: **Radiographic Positioning**. 2nd ed. Boston: Little Brown. 1995; 381-385.
32. Clark KC, Whitley AS: **Clark's Positioning in Radiography**. 12th ed. London: Arnold. 2005; 1-37
33. Wiebe S. **Positioning Techniques. Private communication. X-ray Laboratory** July 10th 2006.
34. Mohamed A, Evan M, Belinda S: **An Atlas of Human Osteology**. Saskatoon: Dept. of Anatomy and Cell Biology University of Saskatchewan. 2001; 8-9.
35. Huisman HJ. **Prostate Cancer: Precision of Integrating Functional MR Imaging with Radiation Therapy Treatment by Using Fiducial Gold Markers.** Radiology. 2005; **236**:311-317.
36. Scarbrough TJ, Golden NM, Ting JY, Fuller CD, Wong A, Kupelian PA, Thomas CR Jr. **Comparison of Ultrasound and Implanted Seed Marker Prostate Localization Methods: Implications for Image-guided Radiotherapy.** Int J Radiation Oncol Biol Phys. 2006; **65:**378-387.
37. Howard MA,, Lavelle WE, Dobbs MB, Simonson TM, Granner MA. **A Noninvasive, Reattachable Skull Fiducial Marker System.** Journal of neurosurgery.1995; **83**:372-376.
38. Bravin A: **The Biomedical Programs at the ID17 Beamline of the European Synchrotron Radiation Facility.** Springer Netherlands. 2007**;** 225 - 239.
39. Giacovazzo C, Monaco H.L, Viterbo D, Scordari F, Gilli G, Zanotti G, Catti M: **Fundamentals of Crystallography**. Oxford University Press. 2002; 273-281.
40. Bruker Advanced X-ray solutions. **CAD4/MACH3 User manual for UNIX systems &**

Linux PC's. Nonius BV. 2000; 7-20.

41. Solidwork CAD Program: Dassault Systèmes SolidWorks Corp. 300 Baker Avenue Concord.
42. Evans P R. **Rotations and Rotation Matrix.** Acta Cryst. 2001; **57**:1355-1359.
43. Kaczorek,T **; Polynomial and rational matrices : applications in dynamical systems theory;** London: Springer. 2007; 225-245.

APPENDIX

This chapter gives a full detail of the drawings use in the design of the fiducial subject pre-alignment system as well as some important drawings that pertain to the construction of the C-arm fiducial system.

APPENDIX A

Laser Alignment Procedure

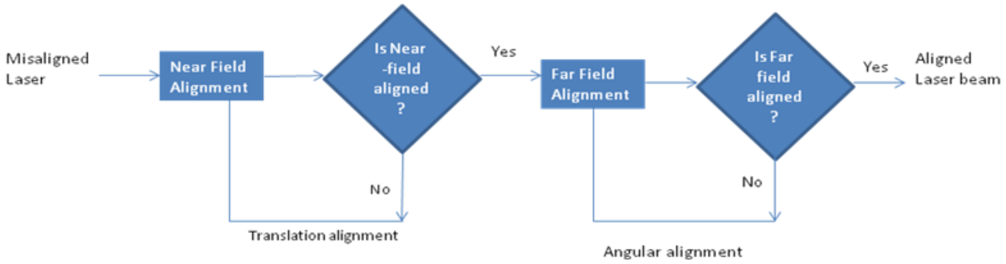

Laser alignment procedure

1. Start from point 1 (origin).
2. Rotate by 180 deg to point 2.
3. Rotate by 90 deg to point 3.
4. Draw a mid- line at point 3 to divide point 1 and 2.
5. Rotate -90 deg back to point 2.
6. Translate from point 2 to mi-point.
7. Then do the final rotation at the mid-point.
8. This aligns the system, and it stays on the axis.
9. Align the laser point with the center of the axis on the other side of the system.

APPENDIX B

Small Straight Mirror Mount

Straight mount offers a 1.50" square mounting surface. Two stainless steel fine-resolution (64-pitch) mounting screws allow precise tilting of this mounting surface in two directions. Unit features various sized mounting holes. Suitable for mounting to most post mounts. Available with or without a 25mm x 35mm, 1/4 wave first surface mirror.

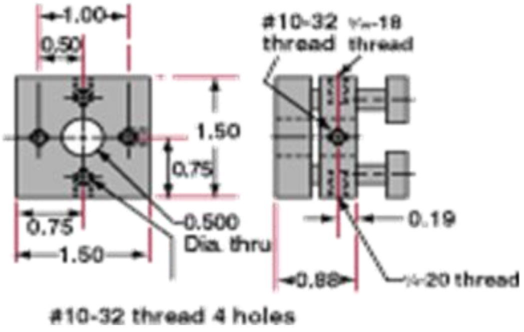

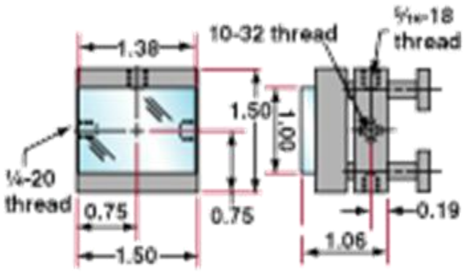

Edmund
optics | worldwide

APPENDIX C

Driven Linear Motion Slide Assemblies

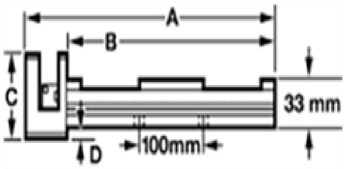

Side View

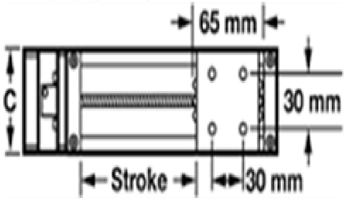

Top View

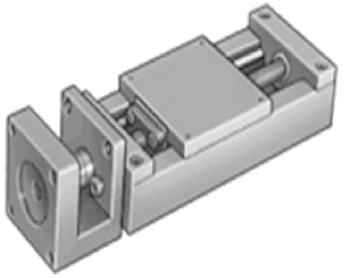

Slides have a wear-compensating acetal nut for smooth, consistent operation and include a flexible helical coupling. Frame and guide block are aluminum. Screw is Type 303 stainless steel. Rails are made of hardened and ground steel. Base has M5 Dia.x 7.9 mm Dp. mounting holes with 9 mm Dia. x 5.5 mm Dp. counterbore.

Straightness accuracy is 0.0001" per inch of travel. Maximum motor input is 2200 rpm. Max. temperature is 185° F.

McMASTER-CARR

APPENDIX D – COMPLETE C-ARM FIDUCIAL SYSTEM AND PARTS

Right view

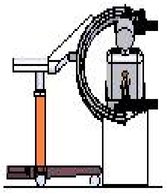

Back view

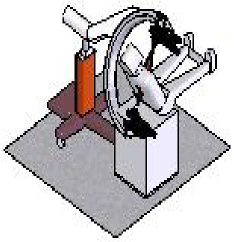

Isometric view

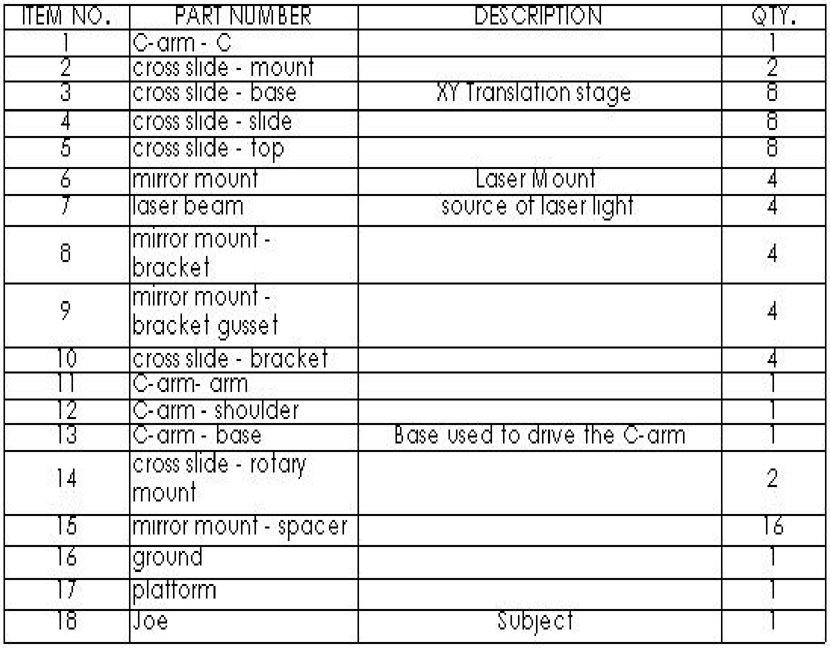

ITEM NO.	PART NUMBER	DESCRIPTION	QTY.
1	C-arm - C		1
2	cross slide - mount		2
3	cross slide - base	XY Translation stage	8
4	cross slide - slide		8
5	cross slide - top		8
6	mirror mount	Laser Mount	4
7	laser beam	source of laser light	4
8	mirror mount - bracket		4
9	mirror mount - bracket gusset		4
10	cross slide - bracket		4
11	C-arm- arm		1
12	C-arm - shoulder		1
13	C-arm - base	Base used to drive the C-arm	1
14	cross slide - rotary mount		2
15	mirror mount - spacer		16
16	ground		1
17	platform		1
18	Joe	Subject	1

All dimesions in mm

Scale: 1:50

APPENDIX E – CROSS SLIDE BASE

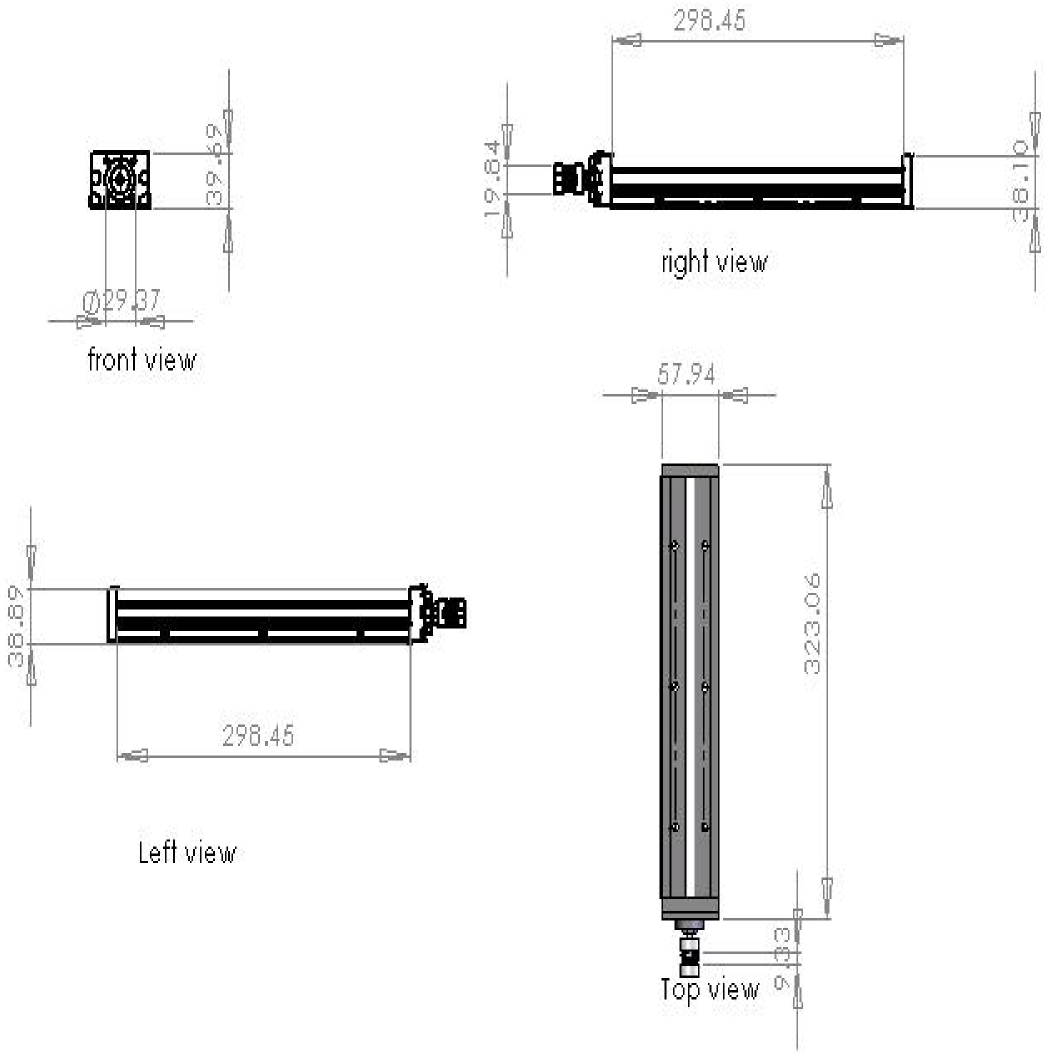

ITEM NO.	PART NUMBER	DESCRIPTION	QTY.
1	cross slide - base	XY Translation stage	1

scale: 1:5

All dimension in mm

APPENDIX F – COMPLETE MRTL SYSTEM AND PARTS

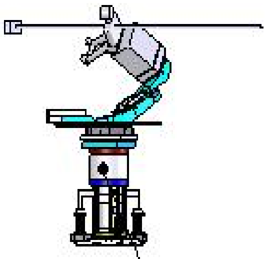

Front view

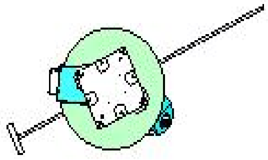

Bottom view

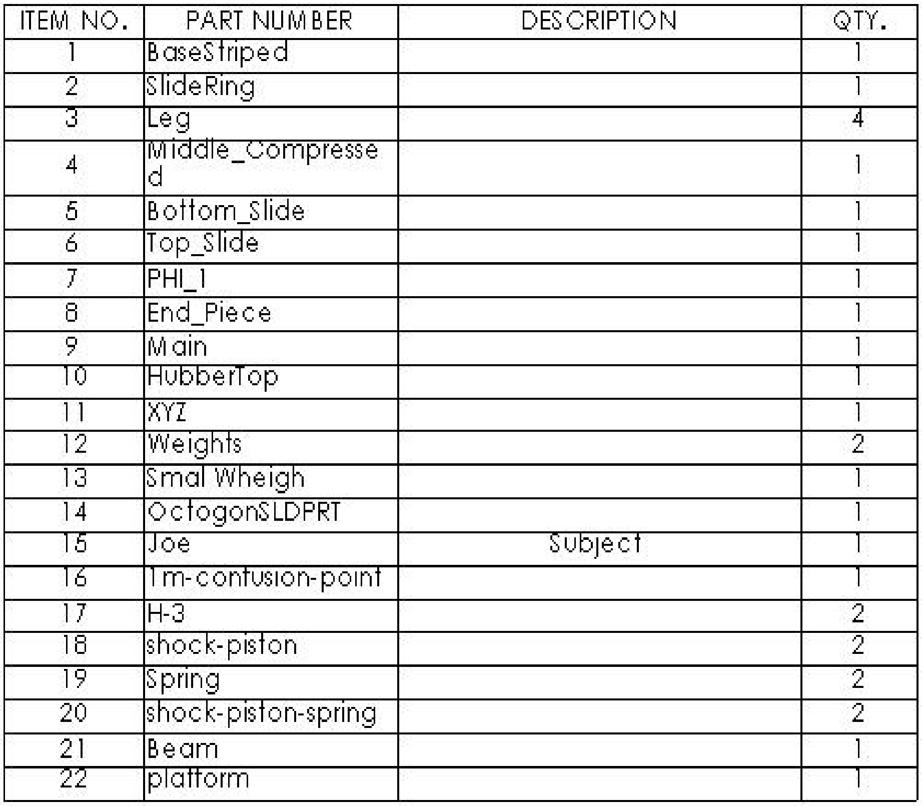

ITEM NO.	PART NUMBER	DESCRIPTION	QTY.
1	BaseStriped		1
2	SlideRing		1
3	Leg		4
4	Middle_Compressed		1
5	Bottom_Slide		1
6	Top_Slide		1
7	PHI_1		1
8	End_Piece		1
9	Main		1
10	HubberTop		1
11	XYZ		1
12	Weights		2
13	Smal Wheigh		1
14	OctogonSLDPRT		1
15	Joe	Subject	1
16	1m-contusion-point		1
17	H-3		2
18	shock-piston		2
19	Spring		2
20	shock-piston-spring		2
21	Beam		1
22	platform		1

Scae: 1:100

All dim. in mm

APPENDIX G – MIRROR MOUNT

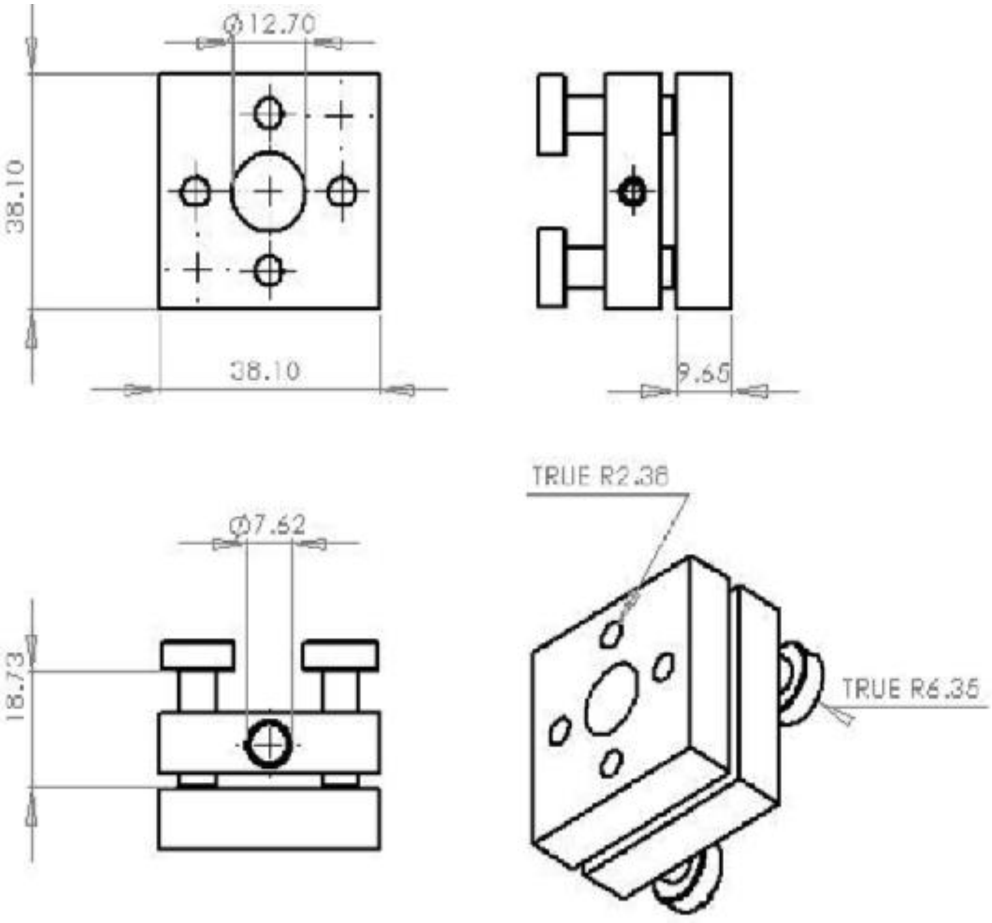

ITEM NO.	PART NUMBER	DESCRIPTION	QTY.
1	mirror mount	All dimensions in *mm*	1

APPENDIX H – C-ARM BASE

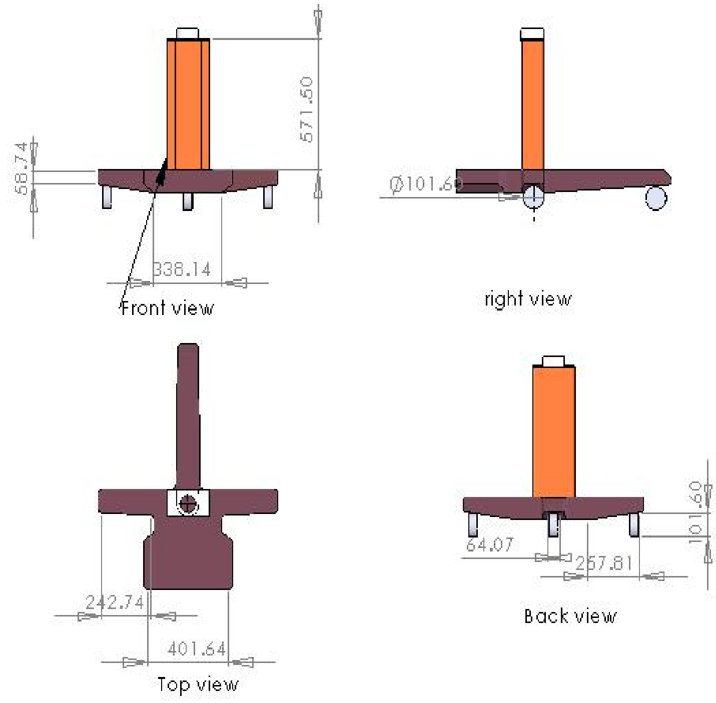

ITEM NO.	PART NUMBER	DESCRIPTION	QTY.
1	C-arm - base	Base used to drive the C-arm	1

Scale: 1:20

All dimensions in mm